A lncRNA identifies *IRF8* enhancer element in negative feedback control of dendritic cell differentiation

Huaming Xu[1,2], Zhijian Li[3], Chao-Chung Kuo[3], Katrin Götz[1,2], Thomas Look[1,2], Marcelo Augusto Szymanski de Toledo[1,2,4], Kristin Seré[1,2], Ivan G. Costa[3] and Martin Zenke[1,2,4*]

[1] Department of Cell Biology, Institute of Biomedical Engineering, RWTH Aachen University Medical School, 52074 Aachen, Germany

[2] Helmholtz Institute for Biomedical Engineering, RWTH Aachen University, 52074 Aachen, Germany

[3] Institute for Computational Genomics, RWTH Aachen University Medical School, 52074 Aachen, Germany

[4] Department of Hematology, Oncology, Hemostaseology, and Stem Cell Transplantation, Faculty of Medicine, RWTH Aachen University, 52074 Aachen, Germany

* **Correspondence:** Martin Zenke, PhD, Department of Cell Biology, Institute for Biomedical Engineering, RWTH Aachen University Hospital, Pauwelsstrasse 30, 52074 Aachen, Germany.
Telephone: +49-241-80 80759; Fax: +49-241-80 82008
email: martin.zenke@rwth-aachen.de

Present addresses:
CCK: Interdisciplinary Centre for Clinical Research (IZKF) Aachen, RWTH Aachen University Medical School, 52074 Aachen, Germany
KG and KS: Department of Cell and Tumor Biology, RWTH Aachen University Medical School, 52074 Aachen, Germany
TL: Laboratory for Molecular Neuro-Oncology, Department of Neurology, University Hospital Zurich and University of Zurich, Zurich, Switzerland

Abstract

Transcription factors play a determining role in lineage commitment and cell differentiation. Interferon regulatory factor 8 (IRF8), a hematopoietic transcription factor, is prominently upregulated in dendritic cells (DC) by autoactivation and controls DC differentiation and function. However, it is unclear how *IRF8* autoactivation is controlled and eventually limited. Here we identified a novel long non-coding RNA transcribed from the +32 kb enhancer downstream of *IRF8* transcription start site and expressed specifically in plasmacytoid DC (pDC), referred to as *lncIRF8*. A sequence element of the *lncIRF8* promoter, but not *lncIRF8* itself, is crucial for pDC and classical DC type 1 (cDC1) differentiation. In DC development *IRF8* autoactivation is first initiated by flanking enhancers and then second controlled by feedback inhibition through the *lncIRF8* promoter element in the +32 kb enhancer. Our work reveals a previously unrecognized negative feedback loop of *IRF8* that orchestrates its own expression and thereby controls DC differentiation.

Key Words: Interferon regulatory factor 8, IRF8, dendritic cell, enhancer, lncRNA, autoactivation feedback loop, CRISPR/Cas9, CRISPR activation, CRISPR interference

Introduction

Lineage-determining transcription factors (TF) are master regulators of gene programs that frequently initiate self-reinforcing loops by autoactivation. TF autoactivation is important for cells to pass restriction points during development (referred to as points of no return) and to enforce cellular identity. Molecular circuitries of autoactivation have been studied for several TF, such as GATA-binding factor 1 (GATA1), PU.1 (encoded by Spi1), CCAAT enhancer-binding protein α and ε (C/EBPα and ε) (Graf and Enver, 2009; Loughran et al., 2020; Nishimura et al., 2000; Okuno et al., 2005; Theilgaard-Mönch et al., 2022). A further example is interferon regulatory factor 8 (IRF8), which shows autoactivation in cooperation with basic leucine zipper ATF-like transcription factor 3 (Batf3) (Anderson et al., 2021; Grajales-Reyes et al., 2015). An important principle in nature is negative feedback control to avoid signal overshooting and toxicity. Negative feedback control applies also to lineage-determining TF, however there is a paucity on our knowledge of the molecular mechanisms involved.

IRF8 is a hematopoietic TF positioned at the center of the regulatory gene network for dendritic cell (DC) development (Anderson et al., 2021; Chauvistré and Seré, 2020; Lin et al., 2015; Nutt and Chopin, 2020; Tamura et al., 2015; Verlander et al., 2022). *IRF8* knockout mice show abnormal development of classical DC type 1 (cDC1) and plasmacytoid DC (pDC) (Durai et al., 2019; Schiavoni et al., 2002; Sichien et al., 2016; Tsujimura et al., 2003). *IRF8* is prominently upregulated during DC development by autoactivation (Grajales-Reyes et al., 2015; Lin et al., 2015), yet how *IRF8* autoactivation is controlled and eventually limited, and the epigenetic mechanisms involved is largely unknown.

IRF8 expression in hematopoietic cells is induced and maintained by enhancers located at -50 kb, +32 kb, +41 kb and +56 kb relative to *IRF8* transcription start site (TSS) (Anderson et al., 2021; Bagadia et al., 2019; Durai et al., 2019; Grajales-Reyes et al., 2015; Murakami et al., 2021; Schönheit et al., 2013). Enhancers regulate complex gene networks and can also produce non-coding RNA, referred to as enhancer RNA (eRNA). eRNA serve as an indicator for enhancer activity and some eRNA have an activity on their own and act in cis or trans to regulate cell fate decisions (Sartorelli and Lauberth, 2020; Statello et al., 2021). Enhancer-associated long non-coding RNA (lncRNA) represent a class of lncRNA transcribed from active enhancers. Thus, eRNA and enhancer-associated lncRNA provide opportunities to detect enhancer activity and to investigate enhancer function.

DC are highly specialized immune cells that play a critical role in regulating innate and adaptive immune responses (Cabeza-Cabrerizo et al., 2021). DC develop from hematopoietic stem cells (HSC) via successive steps of lineage commitment and differentiation. More specifically, HSC develop into multipotent progenitors (MPP) that are committed to DC restricted common DC progenitors (CDP) and differentiate into classic DC (cDC) type 1 and type 2 (cDC1 and cDC2, respectively) and pDC (Anderson et al., 2021; Cabeza-Cabrerizo et al., 2021; Nutt and Chopin, 2020; Rodrigues and Tussiwand, 2020). pDC were recently also shown to develop from lymphoid progenitors (Dress et al., 2019; Rodrigues et al., 2018; Rodrigues and Tussiwand, 2020). Differential expression of *IRF8* regulates DC and monocyte specification in a dose-dependent manner (Cytlak et al., 2020; Murakami et al., 2021). *IRF8* expression

starts at the CDP stage, and is high in pDC and cDC1, which is attributed to the autoactivation of *IRF8* during DC subsets specification (Grajales-Reyes et al., 2015; Lin et al., 2015). Interestingly, IRF8 can act as a transcriptional activator or repressor in hematopoiesis by interacting with different partner TF and binding to specific DNA sequences (Tamura et al., 2015).

As an activator, IRF8 binds to its own promoter in DC differentiation, which is considered as the autoactivation capacity of *IRF8* (Grajales-Reyes et al., 2015; Lin et al., 2015). For instance, IRF8 interacts with partner TF, such as PU.1, to initiate *IRF8* autoactivation at the CDP stage (Grajales-Reyes et al., 2015). Inversely, IRF8 inhibits C/EBPα activity in neutrophil differentiation (Kurotaki et al., 2014). IRF8 also represses C/EBPβ to generate and maintain DC lineage-specific enhancer landscapes (Bornstein et al., 2014). In addition, IRF8 is important for the *Myc-Mycl* transition in DC differentiation (Anderson III et al., 2021). IRF8 represses *Myc* expression in progenitors, while IRF8 at high levels interacts with PU.1 and drives *Mycl* expression (Anderson III et al., 2021). All this emphasizes the central position of IRF8 in coordinating the gene network that regulates DC differentiation and function.

During DC differentiation, the *IRF8* gene locus shows high epigenetic dynamics, including histone modifications and TF binding identified by ChIP-seq (Chauvistré and Seré, 2020; Durai et al., 2019; Grajales-Reyes et al., 2015; Lin et al., 2015), chromatin accessibility measured by ATAC-seq (Kurotaki et al., 2019; Li et al., 2019), and three-dimensional chromatin structure remodeling determined by chromosome conformation capture (3C) (Schönheit et al., 2013). All this emphasizes the impact of epigenetic regulators on *IRF8* gene activity in DC differentiation. Notably, *IRF8* is flanked by multiple enhancers at -50 kb, +32 kb, +41 kb and +56 kb that regulate *IRF8* expression in hematopoietic cells (Anderson et al., 2021; Murakami et al., 2021). These four enhancers were found to be driven by PU.1, Batf3, E proteins and Runt-related transcription factor (RUNX)-core binding factor beta (CBFβ) (RUNX-CBFβ), respectively (Bagadia et al., 2019; Durai et al., 2019; Grajales-Reyes et al., 2015; Murakami et al., 2021; Schönheit et al., 2013).

Chromatin conformation, particularly enhancer-promoter interactions, provides a platform for TF-driven gene regulation and serves as a driving force for cell-fate determinations (Misteli and Finn, 2021; Oudelaar and Higgs, 2021; Stadhouders et al., 2019). Schönheit et al. demonstrated *IRF8* promoter interactions with its upstream enhancers by quantitative 3C (Schönheit et al., 2013). In this study PU.1 was found to regulate chromatin remodeling between the -50 kb enhancer and the *IRF8* promoter in myeloid differentiation. Thus, while the Schönheit et al., 2013 study represents a good starting point, it has remained of great importance to unveil the physical chromatin interactions of the *IRF8* promoter with upstream and downstream enhancers on a large scale and at high resolution to understand *IRF8* regulation during DC differentiation (Murakami et al., 2021).

Frequently, chromatin data, including ATAC-seq and/or ChIP-seq data, are used to identify regulatory elements of gene transcription. Here we embarked on a different approach and searched for lncRNA, which by themselves might have regulatory functions or are indicative of enhancer activity. We identified

a novel lncRNA transcribed from the *IRF8* +32 kb enhancer, which is specifically expressed in pDC, referred to as *lncIRF8*. We found that the *lncIRF8* promoter element but not *lncIRF8* itself impacts pDC and cDC1 development. Thus, *lncIRF8* acts as an indicator for the *IRF8* +32 kb enhancer activity. Importantly, our study revealed a previously unrecognized negative feedback loop of *IRF8* in DC differentiation. *IRF8* first activates its expression by autoactivation via the +32 kb enhancer and second limits its own expression through the *lncIRF8* promoter element in the +32 kb enhancer.

Results

lncIRF8 marks a pDC specific *IRF8* enhancer element

IRF8 expression in DC development is subject to complex epigenetic regulation. Here we used an integrated approach with RNA-seq, ATAC-seq, ChIP-seq and Capture-C to track the dynamics of gene expression, histone modification and chromatin conformation in the sequel MPP, CDP, pDC, cDC1 and cDC2 (Figure 1, Figure S1 and Figure S2A).

We performed de-novo transcript assembly of the RNA-seq data and detected two previously unknown transcripts without coding potential downstream of *IRF8*: a pDC specific lncRNA (*TCONS_00190250*) in the following referred to as *lncIRF8* and a cDC1 specific lncRNA (*TCONS_00190258*; Figure 1A and Figure S1). *lncIRF8* is transcribed within an enhancer region located 32 kb downstream of the *IRF8* TSS labeled by H3K27ac and H3K4me1 and occupied by DC differentiation-associated TF, such as IRF8 and PU.1 (Figure 1A and Figure S1). This region is largely devoid of H3K9me3, a chromatin modification frequently associated with heterochromatin, indicating an open chromatin configuration in DC (Figure S1). In addition, sequences of this region have been implicated in DC development and referred +32 kb enhancer (Durai et al., 2019). Thus, we proceeded to study *lncIRF8* in detail.

ATAC-seq analysis revealed further details of the *lncIRF8* region in CDP, pDC, cDC1 and cDC2 (Figure 1A, Figure 2A and Figure S1). In cDC1 the prominent ATAC-seq and IRF8 peaks mark the cDC1 specific +32 kb enhancer (Durai et al., 2019). In pDC the ATAC-seq peak is smaller and shifted further towards downstream but aligns well with the valley in the prominent H3K27ac peak. This ATAC-seq peak marks the *lncIRF8* promoter and aligns with p300 and H3K4me3 (Figure 2A and Figure S1) (Durai et al., 2019). All this indicates that this chromatin region is open and transcriptionally active in pDC, enabling *lncIRF8* transcription.

Next, we determined the chromatin conformation of the *IRF8* locus and the *lncIRF8* region. We generated interaction profiles by nuclear-titrated (NuTi) Capture-C in MPP, CDP, pDC, cDC1 and cDC2 (Figure S2A and B) using *IRF8* promoter as viewpoint. The *IRF8* promoter shows multiple interactions with regions spanning up to ~100 kb upstream and downstream of *IRF8* (Figure 1B and Figure S1). In pDC the *IRF8* promoter interactions are stronger with the upstream sequences than with downstream sequences (Figure 1C and Figure S2C). In cDC1 *IRF8* promoter interactions are more confined to the regions downstream of *IRF8* compared to MPP, CDP and pDC (Figure 1C, Figure S2C). This suggests that upstream and downstream sequences of *IRF8* gene are involved in differentially regulating *IRF8* expression and controlling the development of pDC and cDC1, respectively.

The CCCTC-binding factor (CTCF) is important for regulation of chromatin conformation through loop extrusion (Sanborn et al., 2015) and we therefore visualized CTCF binding sites in the *IRF8* locus in DC (Garber et al., 2012). Interestingly, most of the *IRF8* flanking enhancers (Durai et al., 2019; Grajales-Reyes et al., 2015; Murakami et al., 2021; Schönheit et al., 2013) are located within convergent CTCF binding sites upstream and downstream of the *IRF8* gene (Figure 1B and Figure S1). There are also

multiple interactions within this region without convergent CTCF binding sites, suggesting interactions with *IRF8* promoter in a CTCF independent manner, such as by TF binding, active histone modifications and gene transcription (Figure 1B and Figure S1) (Owens et al., 2022).

Surprisingly, in pDC H3K27ac at the *lncIRF8* promoter is high, but this locus shows less interactions with the *IRF8* promoter in pDC compared to CDP, cDC1 and cDC2 (Figure 1C and Figure S2C). In addition, in pDC the IRF8 protein occupancy at the *lncIRF8* promoter is low and much higher in cDC (Figure 1A and Figure S1) (Durai et al., 2019; Grajales-Reyes et al., 2015). These observations warrant further studies and we thus proceeded to investigate the *lncIRF8* locus in detail.

***lncIRF8* promoter KO compromises pDC and cDC1 development**

First, we annotated *lncIRF8*. Our de-novo transcript assembly of RNA-seq data revealed different isoforms of *lncIRF8*, with the most prominent isoform comprising exon 2 and 3 (Figure 1A, Figure 2A and Figure S1). Additionally, 3' end and 5' end RACE PCR confirmed the anatomy of this *lncIRF8* isoform: two exons, one intron, and a polyA tail (Figure 2A). Then second, we deleted 300 bp in the *lncIRF8* promoter by CRISPR/Cas9 editing in conditionally immortalized HoxB8 MPP (Figure 2A and Figure S3A-D). The *lncIRF8* promoter is located in the *IRF8* +32 kb enhancer region and is in close proximity to the cDC1 specific +32 kb enhancer (Durai et al., 2019) (Figure 2A and Figure S4). The 300 bp deletion comprises the H3K4me3 promoter mark and is confined to open chromatin identified by ATAC-seq and positioned in the valley of the H3K27ac mark (Figure 2A). Additionally, it contains binding sites for IRF8, PU.1, and Batf3 TF, which are important for DC development (Figure 2A and Figure S4B).

Generation of a precise deletion requires clonal cell populations, which is hardly achieved in somatic cells due to their limited life span. Therefore, we developed a Mx-Cas9-GFP system of conditionally immortalized HoxB8 MPP, which upon differentiation faithfully recapitulate DC development (Figure S3A and B) (Xu et al., 2021). HoxB8 MPP were obtained from bone marrow of Mx-Cas9-GFP mice by infection with the estrogen (E2) inducible HoxB8-ER. These HoxB9 MPP exhibited an extended lifespan and robust clonogenic potential and differentiated into all DC subsets *in vitro* and *in vivo* (Xu et al., 2021). Infection of gRNA targeting *lncIRF8* promoter in Mx-Cas9-GFP HoxB8 MPP and induction of Cas9 by interferon generated single-cell *lncIRF8* promoter KO clones. Five out of 71 single-cell colonies with homozygous deletions were further studied and subjected to DC differentiation (Figure 2C-E, Figure S3C-G, Figure S5A-I).

lncIRF8-promoter KO abolished *lncIRF8* expression during DC differentiation compared to control without deletion (Figure 2B). Surprisingly, *IRF8* expression was also severely compromised, which points to a cross-talk of the *lncIRF8* promoter element with the *IRF8* promoter. To determine whether *lncIRF8*-promoter KO also impacts DC subsets, $CD11c^+$ DC, pDC and cDC subsets cDC1 and cDC2 were analyzed (Figure 2C and Figure S3E-G). Frequencies of pDC and cDC1 were severely reduced, while cDC2 were unaffected (Figure 2C). Accordingly, *lncIRF8*-promoter KO cultures contained mainly

cDC2 and some undifferentiated cells and were more homogenous compared to control without deletion, which contain multiple DC subsets (Figure 2C and D, Figure S3F).

lncIRF8-promoter KO affected also the differentiation propensity of progenitors upon E2 withdrawal from MPP/CDP culture (Figure S2A and Figure S5A-I). *lncIRF8*-promoter KO showed a marked increase in strongly adhesive cells compared to control (Figure S5B). *lncIRF8*-promoter KO cultures had higher frequencies of $Gr1^+$ monocytes (Figure 2E, Figure S5H and I) and lower frequencies of all DC subsets $CD11c^+$ DC, pDC, cDC1, and cDC2 (Figure S5C-G) compared to control without deletion.

We then investigated the impacts of *lncIRF8* promoter KO on DC differentiation *in vivo* and transplanted CD45.2 *lncIRF8*-promoter KO and CD45.2 control HoxB8 MPP into irradiated CD45.1 recipient mice (Figure S5J). DC in bone marrow and spleen were analyzed by flow cytometry on day 7 and 14 after cell transplantation (Figure 3, Figure S5J and K).

In bone marrow, *lncIRF8*-promoter KO cells mostly differentiated into $Gr1^+$ monocytes, and lower frequencies of all DC subsets were observed on day 7 for *lncIRF8*-promoter KO cells compared to control (Figure 3A-F). In spleen, frequencies of cell populations from *lncIRF8*-promoter KO and control were similar to bone marrow, including lower frequencies of all DC subsets for *lncIRF8*-promoter KO (Figure 3G-L). CD45.2 donor HoxB8 cells were largely lost at day 14 after cell transplantation (Figure 3B-F and Figure 3H-L). Thus, *lncIRF8* promoter KO compromised pDC and cDC1 development both *in vitro* and *in vivo*.

lncIRF8 acts as an indicator of _IRF8_ +32 kb enhancer activity in pDC

Knockout of *lncIRF8* promoter and thus abolishment of *lncIRF8* expression severely diminished pDC and cDC1 development *in vitro* and *in vivo*. The *lncIRF8* promoter is located within *IRF8* +32 kb enhancer (Durai et al., 2019) and thus it was important to determine whether *lncIRF8* itself plays a role in regulating pDC and cDC1 development. To address this question, we (i) overexpressed *lncIRF8* in wild-type MPP and (ii) re-expressed *lncIRF8* in *lncIRF8*-promoter KO MPP and monitored its impact on DC development (Figure 4 and Figure S6).

lncIRF8 cDNA was cloned into a polyA lentivirus vector. An "AATAAA" stop signal (Alvarez-Dominguez et al., 2015) was inserted at the 3' end of *lncIRF8* to avoid longer transcripts than *lncIRF8* (p*lncIRF8*-pA, Figure 4B). The respective pGFP-pA vector was used as control. *lncIRF8* overexpressing single-cell clones were generated by limiting dilution (Figure S6A), expanded and subjected to DC differentiation. As expected *lncIRF8* expression was markedly increased in p*lncIRF8*-pA infected cells compared to control, while there were no significant differences in *IRF8* expression between the two groups during DC differentiation (Figure 4C). Further, there were no differences in the frequencies of pDC, cDC1, and cDC2 between p*lncIRF8*-pA infected cells and controls (Figure 4D and E, Figure S6B-D), indicating that *lncIRF8* overexpression has no effect on *IRF8* expression and DC differentiation.

To further extend this observation we performed a *lncIRF8* rescue in *lncIRF8* promoter KO MPP. *lncIRF8* was re-expressed in *lncIRF8*-promoter KO MPP by lentiviral vector and cells were subjected to DC differentiation (Figure S6E). *lncIRF8* RNA was effectively expressed and cells differentiated in response to Flt3L (Figure S6F). Yet frequencies of pDC and cDC1 were very low to absent and not rescued by *lncIRF8* expression (Figure S6G and H).

In a nutshell, *lncIRF8* overexpression and rescue had no effects on pDC and cDC1 development. This strongly suggests that *lncIRF8* has no activity on its own in DC differentiation but rather acts as an indicator for the activation state of sequences within the *IRF8* +32 kb enhancer. In addition, the *lncIRF8* promoter comprises a sequence element with impact on pDC and cDC1 development.

Activation of *lncIRF8* promoter promotes cDC1 development

Next, we proceeded to study the impact of the sequence element within *lncIRF8* promoter on *IRF8* expression and DC differentiation using CRISPR activation by dCas9-VP64 (Figure 5A). dCas9-VP64 is a mutated Cas9 deficient in nuclease activity, which is fused to the VP64 effector domain and confers gene activation. Targeting of dCas9-VP64 to the *lncIRF8* promoter was achieved with specific gRNAs (Figure S7I). We also included targeting dCas9-VP64 to the *IRF8* promoter to study the interplay with the *lncIRF8* promoter. FACS sorted HoxB8 MPP expressing dCas9-VP64 and gRNA were subjected to DC differentiation (Figure S7A) and analyzed for *lncIRF8* and *IRF8* expression and DC subset composition (Figure 5B-E).

Activation of the *lncIRF8* promoter by dCas9-VP64 caused a massive increase of *lncIRF8* expression at DC differentiation day 0 (Figure 5C). The activation of the *lncIRF8* promoter led also to *IRF8* upregulations at DC differentiation day 5, 7, and 9 compared to non-targeting control (Figure 5A and C). This demonstrates the positive impact of the *lncIRF8* promoter element on *IRF8* expression during DC differentiation and is in accord with the physical interaction of *lncIRF8* and *IRF8* promoters by Capture-C (Figure 1B and Figure S1).

Intriguingly, in *lncIRF8*-VP64 cells *lncIRF8* expression was downregulated at DC differentiation day 5, 7 and 9, while *IRF8* expression was upregulated (Figure 5C). This indicates a repressive effect of IRF8 on *lncIRF8* promoter and is in accord with IRF8 binding to the *lncIRF8* region by ChIP-seq (Figure 1 and Figure S1). This observation suggests a negative feedback loop of IRF8 on the *lncIRF8* promoter during DC differentiation (Figure 5C).

Activation of *IRF8* promoter by dCas9-VP64 increased *IRF8* expression at DC differentiation day 0, 5, 7, and 9, while expression of *lncIRF8* was unaffected compared to non-targeting control (Figure 5A and C). As expected *IRF8* promoter activation led to higher pDC frequencies (Figure 5B and D), and also increased cDC1 frequencies compared to the non-targeting controls (Figure 5B and E). Importantly, *lncIRF8* promoter activation by dCas9-VP64 also increased cDC1 frequencies and this was particular

prominent at day 9 of DC differentiation (Figure 5B and E). Frequencies of cDC2 were decreased at day 9 and other populations, including pDC, remained unchanged (Figure 5B and D, Figure S7C-E).

Taken together our CRISPR activation of the *lncIRF8* and *IRF8* promoters by dCas9-VP64 suggest a negative feedback loop of *IRF8* for pDC and cDC1 development.

Negative feedback regulation of *lncIRF8* and *IRF8* promoters controls DC differentiation

To directly investigate the negative feedback loop of *IRF8* regulation, we repressed *lncIRF8* and *IRF8* promoters by targeted repression with dCas9-KRAB and analyzed the DC subsets during DC differentiation (Figure 6A-F). dCas9-KRAB is a nuclease deficient Cas9 fused to the KRAB effector domain, which confers gene repression when positioned with specific gRNA (Figure S7I).

Targeted repression of the *IRF8* promoter decreased *IRF8* expression as expected but massively increased *lncIRF8* expression compared to non-targeting control (Figure 6A and C). This is very much in line with *IRF8* impacting *lncIRF8* expression by a negative feedback loop. Positioning the dCas9-KRAB repressor in the Inc*IRF8* promoter led to downregulation of both *IRF8* and *lncIRF8* expression, which confirms the *lncIRF8* promoter element acting on the *IRF8* promoter (Figure 6A and C).

Interestingly, targeted repression of the *IRF8* promoter severely compromised development of all DC subsets, including pDC, cDC1 and cDC2, compared to non-targeting controls and yielded CD11c^{+} cells with progenitor-like spherical morphology (Figure 6B, D-F, Figure S7F-H). This reemphasizes the pivotal role of IRF8 for DC development known from studies on *IRF8* knockout mice (Murakami et al., 2021; Schiavoni et al., 2002; Sichien et al., 2016; Tsujimura et al., 2003). In addition, targeted repression of the *lncIRF8* promoter (*lncIRF8*-KRAB) also compromised pDC and cDC1 development (Figure 6B, D and E). This result is very similar to the *lncIRF8* promoter KO analyzed above (Figure 2A-C).

All these findings support a model of *IRF8* regulating its own expression by a negative feedback loop acting on the *IRF8* +32 kb enhancer to limit *IRF8* autoactivation (Figure 7). This regulatory *IRF8* +32 kb enhancer element is marked by *lncIRF8*. *IRF8* expression starts in CDP and further increases in pDC and cDC1, with particularly high expression in pDC (Figure 1A and Figure S1). The increase in *IRF8* expression is proposed to be due to an increase in the interactions of the *IRF8* promoter with upstream and downstream sequences. In pDC the *IRF8* promoter-enhancer interactions are more with upstream chromatin regions (Figure 1C), which relates to high *IRF8* expression. In cDC1 the *IRF8* promoter interactions are stronger with the regions downstream of *IRF8* (Figure 1C) and the *IRF8* +32 kb enhancer marked by *lncIRF8* confers transcriptional repression.

In our model we propose an IRF8 repressor complex that differentially acts on the *IRF8* +32 kb enhancer element in a DC subset specific manner to limit *IRF8* autoactivation. In cDC1 the +32 kb enhancer is repressed by the IRF8 repressor complex through negative feedback inhibition (prominent IRF8 binding

in cDC by ChIP-seq; Figure 7A), which limits *IRF8* autoactivation and expression. Conversely, in pDC there is less IRF8 repressor complex binding to the +32 kb enhancer, which results in high *IRF8* and *lncIRF8* transcription (Figures 7A). Recapitulating the IRF8 repressor complex with dCas9-KRAB and targeting *lncIRF8* promoter in the +32 kb enhancer reduced *IRF8* expression (Figure 7B). Conversely, activation of the +32 kb enhancer boosted *lncIRF8* and *IRF8* expression (Figure 7B). Thus, an intricate feedback loop of IRF8 on the +32 kb enhancer orchestrates *IRF8* expression and thus DC differentiation.

Discussion

Hematopoiesis is a particularly well studied stem cell system and therefore provides an excellent model for studying TF in lineage commitment and cell differentiation, and the molecular principles involved (Graf and Enver, 2009; Laurenti and Göttgens, 2018; Nutt and Chopin, 2020). This work revealed a previously unrecognized negative feedback loop of *IRF8* in DC differentiation and shows how *IRF8* autoactivation is controlled and ultimately limited. IRF8 is crucial for DC lineage specification both in humans and mice (Anderson et al., 2021; Cabeza-Cabrerizo et al., 2021; Cytlak et al., 2020; Kurotaki et al., 2019; Nutt and Chopin, 2020). *IRF8* is upregulated by autoactivation via the +32 kb enhancer (Grajales-Reyes et al., 2015; Lin et al., 2015). However, how *IRF8* expression is controlled at late stages of DC differentiation and eventually limited is not known. Here we demonstrate that *IRF8* expression is limited by a negative feedback loop via a sequence element marked by *lncIRF8* in the *IRF8* +32 kb enhancer.

IRF8 expression in hematopoiesis is regulated by its flanking enhancers, which determine lineage specification and DC subset development (Bagadia et al., 2019; Durai et al., 2019; Grajales-Reyes et al., 2015; Murakami et al., 2021; Schönheit et al., 2013). Frequently, enhancers are identified by ATAC-seq and ChIP-seq (Durai et al., 2019; Murakami et al., 2021), and here we embarked on a different approach and searched for eRNA and enhancer-associated lncRNA by RNA-seq. We identified a novel pDC specific lncRNA (*lncIRF8*) transcribed from the *IRF8* +32 kb enhancer. *lncIRF8* itself lacks activities in DC differentiation but a *lncIRF8* promoter element is crucial for pDC and cDC1 development. Upon deletion of this *lncIRF8* promoter element pDC and cDC1 development was severely compromised, demonstrating that this sequence is important for both pDC and cDC1 development.

We propose a model where *IRF8* expression during DC differentiation is in a first step initiated and activated through flanking enhancers, including the +32 kb enhancer by autoactivation (Grajales-Reyes et al., 2015; Lin et al., 2015) (Figure 7). In a second step the *lncIRF8* promoter element confers feedback inhibition, which limits *IRF8* expression. This feedback inhibition is different for pDC and cDC1, both of which express high levels of *IRF8* (Bornstein et al., 2014; Grajales-Reyes et al., 2015; Lin et al., 2015). In cDC1, *IRF8* expression is attributed to *IRF8* autoactivation through the +32 kb enhancer driven by the Batf3-IRF8 complex (Durai et al., 2019; Grajales-Reyes et al., 2015). In pDC, *IRF8* expression is even higher than in cDC1 (Bornstein et al., 2014; Lin et al., 2015), which we propose is due to less feedback inhibition at late stages of DC differentiation.

A candidate for mediating *IRF8* feedback inhibition is IRF8 itself, since IRF8 works as transcriptional activator or repressor, depending on context. IRF8 activator or repressor function depends largely on the heterodimers (or even heterotrimers) with partner TF that bind to specific DNA sequences (Chang et al., 2018; Huang et al., 2016; Humblin et al., 2017; Tamura et al., 2015; Yoon et al., 2014). Modifications on IRF8 protein, such as phosphorylation and small molecule conjugation, also alter IRF8 activity (Chang et al., 2012; Konieczna et al., 2008). Potential IRF8 heterodimer partners, to form repressor complexes, are ETV6 or IRF2 (Huang et al., 2016; Humblin et al., 2017; Lau et al., 2018).

The IRF8 repressor complex is proposed to bind to the +32 kb enhancer in cDC but not in pDC. This notion is in line with a prominent IRF8 signal at the +32 kb enhancer in cDC, which is absent in pDC (Durai et al., 2019; Grajales-Reyes et al., 2015) (Figure 1A, Figure S1, Figure S4A and Figure 7A).

Further support of our model stems from our CRIPSR activation/interference experiments (Figure 7B). CRIPSR activation of *IRF8* promoter by dCas9-VP64 mimics *IRF8* up-regulation during DC differentiation and causes an increase in pDC and cDC1 (Figure 5). CRIPSR interference of *lncIRF8* promoter by dCas9-KRAB recapitulates transcriptional repressor binding to the +32 kb enhancer and causes *IRF8* promoter inhibition (Figure 6).

We extended our study to delineate the chromatin conformation of the *IRF8* promoter with flanking sequences by Capture-C. The *IRF8* promoter was found to interact with its flanking enhancers already at the CDP stage and then interactions with specific upstream and downstream sequences are proposed to guide pDC and cDC specification, respectively. This is in accord with previous studies where some of these *IRF8* flanking enhancers were required to maintain high levels of *IRF8* expression (Anderson et al., 2021; Murakami et al., 2021).

We demonstrate that deletion of the *lncIRF8* promoter element severely decreased *IRF8* expression and abolished both pDC and cDC1 development *in vitro* and *in vivo* upon cell transplantation. These results are very similar to a previous study on cDC1 specific +32 kb enhancer knockout mice, which demonstrates the impact of +32 kb enhancer for cDC1 development *in vivo* (Durai et al., 2019). The *lncIRF8* promoter is located in close proximity to the cDC1 specific +32 kb enhancer and thus can be expected to have overlapping functions. However, CRISPR deletion and interference of *lncIRF8* promoter compromised both cDC1 and pDC development, while the +32 kb enhancer knockout in mice affected only cDC1 development. The reason for this discrepancy is not clear and could be due to genetic compensation for pDC development in +32 kb enhancer KO mice. Alternatively, the *lncIRF8* promoter element might have additional functions for pDC development, which need to be further addressed.

eRNA and enhancer-associated lncRNA are indicative of enhancer activity, however whether the process of their transcription, the transcripts themselves, or both are functionally linked to enhancer activity, remains unclear (Sartorelli and Lauberth, 2020; Statello et al., 2021). Previous studies revealed that some eRNA and enhancer-associated lncRNA are indeed functionally connected with expression of the respective target genes (Sartorelli and Lauberth, 2020; Statello et al., 2021). Here we found no apparent activity of *lncIRF8* on its own in pDC and cDC1 development, as demonstrated by *lncIRF8* overexpression and rescue experiments. Thus, *lncIRF8* appears to rather serve as an indicator for *IRF8* +32 kb enhancer activity.

In conclusion, by analyzing the gene expression and epigenetic profiles of the *IRF8* locus, we identified an enhancer element marked by *lncIRF8* that regulates *IRF8* and controls DC differentiation through a

negative feedback loop. Our results suggest that *IRF8* regulates itself by its flanking enhancers in DC fate determination: First, *IRF8* induces its expression by autoactivation via flanking enhancers, including the *IRF8* +32 kb enhancer, to initiate DC differentiation, and second limits its expression at late stages via the *lncIRF8* promoter element within the same +32 kb enhancer by feedback inhibition. This molecular principle of feedback inhibition is expected to also apply to other TF and cell differentiation systems.

Acknowledgments

We acknowledge the support of the Interdisciplinary Center for Clinical Research Aachen (IZKF Aachen) FACS Core Facility and Genomics Facility. We thank Magdalena Karpinska and Marieke Oudelaar for help with the Capture-C experiments and analysis, Susanne Schmitz and Paul Wanek for assistance, S. Rose-John for hyper-IL-6, Lisa Weixler and Carmen Schalla for help with enzyme purification, and Thomas Hieronymus for valuable discussion and suggestions.

Part of this work was supported in part by funds from German Research Foundation (DFG) to M.Z. and from the Germany Ministry of Science and Technology (BMBF - Fibromap) and the Interdisciplinary Center for Clinical Research Aachen (IZKF Aachen) from the RWTH Medical Faculty to I.C.. H.X. was supported by a fellowship of China Scholarship Council (CSC) (Grant number 202008080170). M.A.S.T. was funded by CAPES-Alexander von Humboldt postdoctoral fellowship (99999.001703/2014-05) and donation by U. Lehmann.

Author Contributions

H.X. and M.Z. conceived the study. H.X. and K.G. performed the Capture-C and data analysis. Z.L., C.C.K., T.L., and I.G.C. did ATAC-seq, ChIP-seq, RNA-seq and data analysis. H.X., K.G., M.A.S.T., T.L. and K.S. performed molecular cloning, cell culture and mouse experiments. H.X. and M.Z. wrote the manuscript and further edited upon input from all co-authors.

Declaration of Interests

The authors declare no competing interests.

Materials and Methods

Resource Table

Reagent or Resource	Source	Identifier
Antibodies		
B220-APC-Cy7, clone RA3-6B2	Biolegend	103223
CD11b-BV510, clone M1/70	Biolegend	101245
CD11c-PE-Cy7, clone N418	Biolegend	117317
CD115-APC, clone AFS98	eBioscience	17-1152-80
CD117 (c-Kit)- PE-Cy7, clone ACK2	eBioscience	25-1172-82
CD135 (Flt3+)-PE, clone A2F10	eBioscience	12-1351-82
CD19-Biotin, clone 6DS	Biolegend	115503
CD3e-Biotin, clone 145-2C11	eBioscience	13-0031-82
CD45.2-APC-Cy7, clone 104	Biolegend	109823
F4/80-Biotin, clone BM8	Biolegend	123105
Gr1-AF700, clone RB6-8C5	Biolegend	108421
Gr1-PerCP-Cy5.5, clone RB6-8C5	eBioscience	45-5931-80
Ly6C-AF700, clone HK1.4	Biolegend	128023
Ly6G-Biotin, clone 1A8	Biolegend	127603
MHCII-BV785, clone M5/114.15.2	Biolegend	107645
NK1.1-Biotin, clone PK136	eBioscience	14-5941-82
SiglecH-SB600, clone eBio440C	Invitrogen	63-0333-82
Streptavidin-PE-Dazzle594	Biolegend	405247
Ter119-Biotin, clone TER-19	eBioscience	14-5921-82
XCR1-BV421, clone ZET	Biolegend	148216
7-AAD-PerCp-Cy5.5	Thermo Fisher Scientific	A1310
Chemicals, Peptides, and Recombinant Proteins		
β-estradiol (E2)	Sigma-Aldrich	E2758
β-mercaptoethanol (β-ME)	Gibco	31350010
BsmBI-v2	New England Biolabs	R0739S
Calcium chloride ($CaCl_2$)	Merck	1.02382.0500
Chondroitin sulfate sodium salt from shark cartilage (CSS)	Sigma-Aldrich	C4384
cOmplete Mini	Roche	
dATP	New England Biolabs	N0440S
Dimethysulfoxide (DMSO)	Sigma-Aldrich	D8418
Doxycycline hyclate	Sigma-Aldrich	D9891
DpnII	A kind gift from A. Marieke Oudelaar, Max Planck Institute for Multidisciplinary Sciences, Göttingen, Germany. DpnII enzyme with a similar activity is also availabel from New England Biolabs.	R0543M
DMEM	Gibco	41965039
DTT	Thermo Fisher Scientific	20290
EDTA	Gibco	15575-038
Fetal calf serum (FCS)	PAA	A01125-499
Fetal calf serum (FCS)	Gibco	10270106
Formaldehyde (37%)	AppliChem	A0877
Recombinant human Flt3-Ligand (Flt3L)	Peprotech	300-19
Recombinant murine stem cell factor (SCF)	Peprotech	250-03
Human IGF-1 long range	Sigma-Aldrich	85580C
Recombinant IL-6/soluble IL-6 receptor fusion protein	A kind gift from S. Rose-John, Kiel, Germany (Fischer et al., 1997). R&D Systems provides a similar product with the same activity.	9038-SR
HEPES	Sigma-Aldrich	H4034
L-glutamine	Gibco	25030081
M-270 Streptavidin Dynabeads	Invitrogen	65305
$MgCl_2$	Thermo Fisher Scientific	R0971
Mouse interferon α (mIFNα)	Miltenyi Biotec	130-093-131
Murine RNase Inhibitor	New England Biolabs	M0314S

Pancoll human, density 1.077g/ml (Ficoll)	PAN-Biotech	P04-601000
Penicillin/streptomycin	Gibco	15140122
Phenol-Chloroform-Isoamyl alcohol (PCI)	Sigma-Aldrich	77617
Phosphate buffered saline (PBS)	Gibco	10010023
Polybrene (PB, Hexadimethrine bromide)	Sigma-Aldrich	H9268
Q5 high fidelity DNA polymerase	New England Biolabs	M0491L
RPMI 1640	Gibco	31870025
SalI	New England Biolabs	R0138S
Sodium chloride (NaCl)	Merck	7647-15-5
Sodium phosphate dibasic (Na_2HPO_4)	Merck	7558-79-4
Supernatant from Flt3L-producing B16F1 cells (1%)	Homemade. Flt3L from Peprotech has the same activity (1:1000)	300-19
Supernatant from CHO KLS C6 cells expressing soluble murine SCF (1%)	Homemade. Peprotech provides a similar product with the same activity (1:1000).	250-03
SYBR-green fluorescence	Applied Biosystems	4385610
T4 DNA HC ligase	Life Tech	EL0013
Taq DNA polymerase	Homemade	N/A
Taq buffer (10x)	Thermo Fisher Scientific	
Template-switching RT enzyme mix	New England Biolabs	M0466
XhoI	New England Biolabs	R0146S
Critical commercial assays		
Gibson Assembly kit	New England Biolabs	E5510S
High-Capacity cDNA Reverse Transcription Kit	Applied Biosystems	4368814
KAPA Hyper Capture Reagent Kit	Roche	9075828001
NEBNext Ultra II DNA Library Prep Kit for Illumina	New England Biolabs	E7645S
NEBNext Multiplex Oligos for Illumina (Index Primers Set 1)	New England Biolabs	E7335S
NEBNext Multiplex Oligos for Illumina (Index Primers Set 2)	New England Biolabs	E7500S
NucleoSpin RNA kit	Macherey-Nagel	740955.250
PCR clean-up kit	Macherey-Nagel	740609.50
TA cloning kit	Thermo Fisher Scientific	K202020
Deposited data		
ATAC-seq MPP	This paper (GSE198651)	GSM5954328; GSM5954329; GSM5954330
ATAC-seq CDP	This paper (GSE198651)	GSM5954331; GSM5954332; GSM5954333
ATAC-seq cDC1	GSE118221	GSM3321239; GSM3321240
ATAC-seq cDC2	This paper (GSE198651)	GSM5954334; GSM5954335
ATAC-seq pDC	GSE118221	GSM3321241; GSM3321242
Capture-C *IRF8*-P MPP	This paper (GSE198651)	GSM5993812; GSM5993813
Capture-C *IRF8*-P CDP	This paper (GSE198651)	GSM5993814; GSM5993815
Capture-C *IRF8*-P cDC1	This paper (GSE198651)	GSM5993816; GSM5993817
Capture-C *IRF8*-P cDC2	This paper (GSE198651)	GSM5993818; GSM5993819
Capture-C *IRF8*-P pDC	This paper (GSE198651)	GSM5993820; GSM5993821
ChIP-seq CTCF DC	GSE36099	GSM881052
ChIP-seq H3K4me1 MPP	GSE57563	GSM1384935
ChIP-seq H3K4me1 CDP	GSE57563	GSM1384936
ChIP-seq H3K4me1 cDC	GSE57563	GSM1384937
ChIP-seq H3K4me1 pDC	GSE57563	GSM1384938
ChIP-seq H3K4me3 MPP	GSE64767	GSM1384939
ChIP-seq H3K4me3 CDP	GSE64767	GSM1384940
ChIP-seq H3K4me3 cDC	GSE64767	GSM1384941

ChIP-seq H3K4me3 pDC	GSE64767	GSM1384942
ChIP-seq H3K9me3 MPP	GSE64767	GSM1384943
ChIP-seq H3K9me3 CDP	GSE64767	GSM1384944
ChIP-seq H3K9me3 cDC	GSE64767	GSM1384945
ChIP-seq H3K9me3 pDC	GSE64767	GSM1384946
ChIP-seq H3K27ac MPP	GSE73143	GSM1887715; GSM1887716
ChIP-seq H3K27ac CDP	GSE73143	GSM1887717; GSM1887718
ChIP-seq H3K27ac cDC	GSE73143	GSM1887719; GSM1887720
ChIP-seq H3K27ac pDC	GSE73143	GSM1887721; GSM1887722
ChIP-seq IRF8 cDC	This paper (GSE198651)	GSM5954341
ChIP-seq IRF8 pDC	This paper (GSE198651)	GSM5954342
ChIP-seq PU.1 MPP	GSE57563	GSM1384951
ChIP-seq PU.1 CDP	GSE57563	GSM1384952
ChIP-seq PU.1 cDC	GSE57563	GSM1384953
ChIP-seq PU.1 pDC	GSE57563	GSM1384954
RNA-seq MPP	This paper (GSE198651)	GSM5954336
RNA-seq CDP	This paper (GSE198651)	GSM5954337
RNA-seq cDC1	This paper (GSE198651)	GSM5954338
RNA-seq cDC2	This paper (GSE198651)	GSM5954339
RNA-seq pDC	This paper (GSE198651)	GSM5954340
lncIRF8 (*TCONS_00190250*)	This paper	GenBank: ON134061
TCONS_00190258	This paper	GenBank: ON134062
Experimental models: cell lines		
HEK293T	ATCC	https://www.atcc.org
lncIRF8-promoter KO HoxB8 MPP	This paper	N/A
Control HoxB8 MPP	This paper	N/A
p*lncIRF8*-pA HoxB8 MPP	This paper	N/A
pGFP-pA HoxB8 MPP	This paper	N/A
IRF8-VP64 HoxB8 MPP	This paper	N/A
lncIRF8-VP64 HoxB8 MPP	This paper	N/A
Non-targeting-VP64-1 HoxB8 MPP	This paper	N/A
Non-targeting-VP64-2 HoxB8 MPP	This paper	N/A
IRF8-KRAB HoxB8 MPP	This paper	N/A
lncIRF8-KRAB HoxB8 MPP	This paper	N/A
Non-targeting-KRAB-1 HoxB8 MPP	This paper	N/A
Non-targeting-KRAB-2 HoxB8 MPP	This paper	N/A
Experimental models: organisms/strains		
C57BL/6 mice	RWTH Aachen University Hospital	N/A
Mx-Cas9-GFP mice	RWTH Aachen University Hospital	N/A
CD45.1 recipient mice	RWTH Aachen University Hospital	N/A
Oligonucleotides		
5'RACE-TSO GCTAATCATTGCAAGCAGTGGTATCAACGCAGAGTACATrGrGrG	New England Biolabs	IDT; 5'RACE of *lncIRF8*
5'RACE-TSO-Specific CATTGCAAGCAGTGGTATCAAC	New England Biolabs	Eurofins Genomics; 5'RACE of *lncIRF8*
5'RACE-GSP-*lncIRF8*-R1 TGTCAGTGATGGGGGCTGGAGAAAT	This paper	
5'RACE-GSP-*lncIRF8*-R2 GCTCAGGATGCCAGGTCCCTTCTT	This paper	
3'RACE-QT CCAGTGAGCAGAGTGACGAGGACTCGAGCTCAAGCTTTTTTTTTTTTTTTT	(Scotto-Lavino et al., 2006)	Eurofins Genomics; 3'RACE of *lncIRF8*
3'RACE-Q0 CCAGTGAGCAGAGTGACG	(Scotto-Lavino et al., 2006)	
3'RACE-QI GAGGACTCGAGCTCAAGC	(Scotto-Lavino et al., 2006)	
3'RACE-GSP-*lncIRF8*-F1 ATTTCTCCAGCCCCCATCACTGACA	This paper	
3'RACE-GSP-*lncIRF8*-F2 AAGAAGGGACCTGGCATCCTGAGC	This paper	

lncIRF8-F TCCTGAAGGGACAGGCAAG	This paper	Eurofins Genomics; *lncIRF8*-promoter KO genotyping
lncIRF8-R CTTGGACATTGAGGACGCC	This paper	
Sc-*lncIRF8*-F ACACTCGAGACTGTCAGATGCAGGGG	This paper	Eurofins Genomics; *lncIRF8* sub-clone
Sc-*lncIRF8*-R AAAAAAGTCGACGCATCAGATTTAATATAGAACTAGGACA	This paper	
CMV-*lncIRF8*-F TGGGCGTGGATAGCGGTTT	This paper	Eurofins Genomics; pGFP-pA and p*lncIRF8*-pA cell line screening
CMV-*lncIRF8*-R CACTGAGACTTAGCAAGGGGGA	This paper	
CMV-GFP-F TGGGCGTGGATAGCGGTTT	This paper	
CMV-GFP-R TGGGGGTGTTCTGCTGGTAG	This paper	
m*lncIRF8*-tQ-F ACTGTCAGATGCAGGGG	This paper	Eurofins Genomics; RT-qPCR for mouse *lncIRF8*
m*lncIRF8*-tQ-R TCACAATCGTCTGTAACTCCG	This paper	
m*IRF8*-tQ-F GAGCGAAGTTCCTGAGATGG	This paper	Eurofins Genomics; RT-qPCR for mouse *IRF8*
m*IRF8*-tQ-R TGGGCTCCTCTTGGTCATAC	This paper	
m*GAPDH*-tQ-F ACCTGCCAAGTATGATGACATCA	This paper	Eurofins Genomics; RT-qPCR for mouse *GAPDH*
m*GAPDH*-tQ-R GGTCCTCAGTGTAGCCCAAGAT	This paper	
m3C-F GGAGAAAGAAGGCTGGTGTTAT	(Downes et al., 2021; Downes et al., 2022)	Eurofins Genomics; qPCR for DpnII digestion efficiency of 3C samples
m3C-R TATCTGAGTTGGACAGCATTGG	(Downes et al., 2021; Downes et al., 2022)	
m3C-control-F TTATCTTGCATTTGCCAACTCG	(Downes et al., 2021; Downes et al., 2022)	
m3C-control-R TGGGTTTCCCTGATTCTGAAA	(Downes et al., 2021; Downes et al., 2022)	
*IRF8*_P_L GATCCGTGCATCACCAGCCTCCTTGACCTTAGGCAGACGCCCCAGCCCCCCGGCCATTTTTGGGGCAGCC	This paper	Sigma-Aldrich; 3C probes targeting *IRF8* promoter
*IRF8*_P_R CCAAATGAACAAACACCTCTCCCTTTAAAATCTGCCTGATGGCCAACTTCATAATGAAGAGAAATAGATC	This paper	
gRNA-1-F CACCGTCCATTATACTAAGATACCC	This paper	Eurofins Genomics; *lncIRF8* promoter KO
gRNA-1-R AAACGGGTATCTTAGTATAATGGAC	This paper	
gRNA-2-F CACCGGTGCCGAGAAAGGACACGT	This paper	
gRNA-2-R AAACACGTGTCCTTTCTCGGCACC	This paper	
gRNA-*IRF8*-VP64-F CACCGACGGTCGCGCGAGCTAATTG	This paper	Eurofins Genomics; CRISPR activation of *IRF8*
gRNA-*IRF8*-VP64-R AAACCAATTAGCTCGCGCGACCGTC	This paper	
gRNA-*IRF8*-KRAB-F CACCGCGGCAGGTAGGACGCGATG	This paper	Eurofins Genomics; CRISPR interference of *IRF8*
gRNA-*IRF8*-KRAB-R AAACCATCGCGTCCTACCTGCCGC	This paper	
gRNA-*lncIRF8*-VP64-F CACCGGTGCCGAGAAAGGACACGT	This paper	Eurofins Genomics; CRISPR activation of *lncIRF8*
gRNA-*lncIRF8*-VP64-R AAACACGTGTCCTTTCTCGGCACC	This paper	
gRNA-*lncIRF8*-KRAB-F CACCGAGTCACTCGTCCTTTGGGG	This paper	Eurofins Genomics; CRISPR interference of *lncIRF8*
gRNA-*lncIRF8*-KRAB-R AAACCCCCAAAGGACGAGTGACTC	This paper	
gRNA-non-targeting-1-F CACCGCGAGGTATTCGGCTCCGCG	(Manguso et al., 2017)	

gRNA-non-targeting-1-R AAACCGCGGAGCCGAATACCTCGC	(Manguso et al., 2017)	Eurofins Genomics; CRISPR control
gRNA-non-targeting-2-F CACCGATGTTGCAGTTCGGCTCGAT	(Manguso et al., 2017)	
gRNA-non-targeting-2-R AAACATCGAGCCGAACTGCAACATC	(Manguso et al., 2017)	
Recombinant DNA		
psPAX2	Addgene	#12260
pMD2.G	Addgene	#12259
pLKO5.sgRNA.EFS.tRFP	Addgene	#57823
pLKO5.sgRNA.EFS.tRFP657	Addgene	#57824
pGFP-pA	This paper	Gibson Assembly
p*lncIRF8*-pA	This paper	Standard cloning
dCAS9-VP64_GFP	Addgene	#61422
pTet-KRAB-dCas9-GFP	(Xu et al., 2021)	N/A
Software and Algorithms		
Bowtie2	http://bowtie-bio.sourceforge.net (Langmead and Salzberg, 2012)	N/A
CapCruncher (v0.1.1a1)	https://github.com/sims-lab/CapCruncher (Downes et al., 2022)	N/A
CPAT	http://code.google.com/p/cpat/ (Wang et al., 2013)	N/A
Cufflinks (version 2.0)	http://cufflinks.cbcb.umd.edu/ (Trapnell et al., 2012)	N/A
FlowJo V10	BD Biosciences	N/A
IGV browser	Broad Institute	N/A
MOODS	https://www.cs.helsinki.fi/group/pssmfind/ (Korhonen et al., 2009)	N/A
Oligo	https://oligo.readthedocs.io/en/latest/index.html (Oudelaar et al., 2020)	N/A
PhyloCSF	http://compbio.mit.edu/PhyloCSF (Lin et al., 2011)	N/A
Prism	GraphPad	N/A
Star aligner (version 2.4)	http://code.google.com/p/rna-star/ (Dobin et al., 2013)	N/A
Snapgene	GSL Biotech	N/A

Data and code availability

ATAC-seq (MPP, CDP and cDC2), Capture-C targeting *IRF8* promoter (MPP, CDP, cDC1, cDC2 and pDC), IRF8 ChIP-seq (cDC and pDC), and RNA-seq (MPP, CDP, cDC1, cDC2 and pDC) data generated in this study have been deposited in Gene Expression Omnibus and are accessible through GEO Series accession numbers GSE198651.

ATAC-seq data of cDC1 and pDC (GSE118221) are published (Li et al., 2019), and the ATAC-seq data of MPP, CDP and cDC2 of the same study are described here (GSE198651). ChIP-seq of CTCF in DC (GSE36099) (Garber et al., 2012), H3K27ac (GSE73143) (Allhoff et al., 2016), H3K4me1 and PU.1 (GSE57563) (Allhoff et al., 2014), H3K4me3 and H3K9me3 (GSE64767) (Lin et al., 2015) in MPP, CDP, cDC and pDC were re-analyzed in this study.

The sequence of the pDC specific lncRNA (*lncIRF8* identified by RACE PCR) and the cDC1 specific lncRNA (*TCONS_00190258* identified by RNA-seq) has been submitted to GenBank. The GenBank accession numbers for *lncIRF8* and *TCONS_00190258* are ON134061 and ON134062, respectively.

Animals

Wild type C57BL/6, Mx-Cas9-GFP knock-in mice (Kühn et al., 1995; Platt et al., 2014; Xu et al., 2021), and CD45.1 recipient C57BL/6 mice were used in this study. Mice were kept under specific pathogen-free conditions in the central animal facility of RWTH Aachen University Hospital, Aachen, Germany. All the animal experiments were approved by the local authorities of the German State North Rhine-Westphalia, Germany according to the German animal protection law.

Cell lines and culture

Multipotent progenitors (MPP) were obtained from mouse bone marrow and expanded *in vitro* with a two-step protocol as described in (Felker et al., 2010). Conditionally immortalized HoxB8 MPP were generated by retrovirus infection of bone marrow cells from wild-type or Mx-Cas9-GFP knock-in mice with an estrogen (E2) inducible HoxB8 estrogen receptor (ER) fusion gene (HoxB8-ER) (Redecke et al., 2013; Xu et al., 2021). MPP were grown in RPMI 1640 medium with 10% FCS (Gibco, 10270106), 100 U/ml penicillin/streptomycin, 2 mM L-glutamine and 50 µM β-ME with a four-cytokine cocktail of SCF, Flt3 ligand (Flt3L), IGF-1, and IL-6/soluble IL-6 receptor fusion protein (hyper-IL-6) as before (referred to as MPP growth medium) (Felker et al., 2010; Xu et al., 2021). E2 (1 µM) was added to activate HoxB8-ER and to maintain the conditionally immortalized state of HoxB8 MPP. Cell density was adjusted to 1.5 million cells/ml every day. HEK293T cells for retrovirus and lentivirus production were grown in DMEM supplemented with 10% FCS (PAA, A01125-499), 100 U/ml penicillin/streptomycin, 2 mM L-glutamine.

Methods Details

***In vitro* DC differentiation with HoxB8 MPP**

HoxB8 MPP were differentiated into DC using a two-step protocol modified from (Felker et al., 2010) and described in (Xu et al., 2021). In brief, 0.75 million cells/ml were grown in MPP growth medium with 50 ng/ml Flt3L (Peprotech, 300-19) and reduced E2 (0.01 µM) for two days and cell density was kept to 0.75 million cells/ml. To induce DC differentiation, HoxB8 MPP were then washed with PBS to remove cytokines and E2, and cultured in RPMI 1640 medium supplemented with FCS, penicillin/streptomycin, L-glutamine, β-ME (same concentrations as above), and Flt3L (50 ng/ml, Peprotech) (referred to as DC differentiation day 0). Partial medium changes were performed on differentiation day 3 and 6. Spontaneous DC differentiation of HoxB8 MPP was achieved simply by removing E2 from growth medium (SCF, Flt3L, IGF1 and hyper-IL6), and culturing the cells at 1.5 million cells/ml (Xu et al., 2021).

Nuclear-Titrated (NuTi) Capture-C

Wild-type bone marrow cell-derived MPP, CDP, cDC1, cDC2, and pDC were generated *in vitro* with the two-step protocol as described in (Felker et al., 2010). Cell populations were sorted by BD FACSAria IIu or BD FACSMelody, MPP are Gr1^{-} CD117^{hi} CD135$^{low/-}$, CDP are Gr1^{-} CD117^{int} CD135^{+} CD115^{+}, cDC1 are CD11c^{+} CD11b$^{low/-}$ XCR1^{+}, cDC2 are CD11c^{+} CD11b^{+} XCR1^{-}, pDC are CD11c^{+} CD11b^{-} B220^{+}.

The chromatin conformation capture (3C) library preparation protocol used in this study was modified from (Downes et al., 2021; Downes et al., 2022). MPP, CDP, cDC1, cDC2 and pDC were fixed with formaldehyde (final concentration 2%) and subjected to nuclear isolation according to the protocol in (Downes et al., 2022; Li et al., 2019). Nuclei (15-20 million per sample) were digested with DpnII and DNA fragments were ligated by T4 DNA HC ligase. DNA was extracted and purified with Phenol-Chloroform-Isoamyl alcohol (PCI, 25:24:1). DpnII digestion efficiency was determined by SYBR qPCR with the primers listed in Resource Table and the quality of 3C libraries was investigated by agarose gel (1%) electrophoresis; 3C samples were used only if the DpnII digestion efficiency was more than 70%.

For *IRF8* promoter viewpoint 2 oligonucleotide probes targeting *IRF8* promoter were designed with the design tool Oligo (https://oligo.readthedocs.io/en/latest/index.html). Oligonucleotide probes are positioned adjacent to the DpnII cut sites on a restriction fragment spanning the *IRF8* promoter (chr8:123,259,948-123,260,530) and 70 bp ssDNA biotinylated oligonucleotides were synthetized by Sigma-Aldrich (listed in Resource Table).

To enrich for fragments containing ligation events with *IRF8* promoter viewpoint, NuTi Capture-C was performed as previously described (Downes et al., 2021; Downes et al., 2022). Briefly, the 3C libraries prepared from MPP, CDP, cDC1, cDC2 and pDC were sonicated using Covaris S220 to an average size of ~200 bp using standard settings recommended by the manufacturer (time: 180 s, duty cycle: 10%, peak incident power: 175 W, cycles per burst: 200, temperature: 5-9°C). End repair was performed with the NEBNext Ultra II kit (New England Biolabs, E7645S) using 2 µg of sonicated 3C library in duplicate for each sample. Illumina NEBNext Indices (New England Biolabs, E7500S, and E7335S) were added with a total of 6 cycles of amplification to allow for multiplexing. After this step, duplicates were pooled to increase sample complexity. We enriched samples as per NuTi Capture-C protocol, with two capture rounds in a multiplexed reaction, using 2 µg of each indexed sample as an input for the first capture. The hybridization with biotinylated probes was performed with the KAPA Hyper Capture Reagent Kit (Roche, 9075828001). Each ssDNA biotinylated probe was used at a concentration of 2.9 nM, with a final pool concentration of 5.8 nM, and 4.5 µl of the pooled oligonucleotides were used per sample. Captured DNA was pulled-down with M-270 Streptavidin Dynabeads (Invitrogen, 65305), washed and amplified off the beads with a total of PCR 14 cycles. The DNA obtained after the first capture was used as an input in the second capture round. The experiments were performed for the first and the second biological replicate separately, and then sequenced with NextSeq 550 Illumina System with 300 paired-end or 150 paired-end, respectively.

NuTi Capture-C data analysis

The Capture-C data was analyzed with CapCruncher (v0.1.1a1) pipeline (https://github.com/sims-lab/CapCruncher) in capture mode (Downes et al., 2022). The reads were aligned to the mm9 genome assembly with Bowtie2 (Langmead and Salzberg, 2012), with specific options: -p6--very-sensitive. Viewpoint coordinates used were: chr8:123,259,948-123,260,530, 1000 bp around viewpoint was

excluded. The data were normalized to ~300 kb region around the viewpoint (chr8:123,132,865-123,433,117).

The Capture-C profiles in Figure 1 and Figure S1 show the mean number of unique interactions in two biological replicates, normalized to ~300 kb region around the viewpoint. Differential tracks were created by subtraction of the mean normalized tracks.

ATAC-seq, ChIP-seq and RNA-seq

ATAC-seq analysis of MPP, CDP, cDC1, cDC2, and pDC was performed by Omni-ATAC-seq (Corces et al., 2017) with minor modifications as described in (Li et al., 2019). RNA-seq analysis and ChIP-seq analysis was done as previously described (Allhoff et al., 2016; Lin et al., 2015).

Plasmids

psPAX2 (Addgene #12260) and pMD2.G (Addgene #12259) for lentiviral packaging and envelope expressing plasmids were kind gifts from Didier Trono, EPFL, Lausanne, Switzerland. The gRNA expressing vector pLKO5.sgRNA.EFS.tRFP (Addgene #57823) and pLKO5.sgRNA.EFS.tRFP657 (Addgene #57824) were kind gifts from Benjamin Ebert, Harvard Medical School, Boston, USA (Heckl et al., 2014).

For *lncIRF8* overexpression and rescue, *lncIRF8* cDNA was introduced into polyA containing lentivirus vector pGFP-pA to generate p*lncIRF8*-pA. pGFP-pA was constructed from pCIG3 (Addgene #78264) (Caviness et al., 2014) by Gibson Assembly (New England Biolabs, E5510S) (Gibson et al., 2009). In brief, the WPRE element was removed and a polyA signal "AATAAA" was inserted at the 3' end of GFP to construct pGFP-pA. *lncIRF8* cDNA was sub-cloned into pGFP-pA using XhoI and SalI with the primers shown in Resource Table to obtain p*lncIRF8*-pA. CRISPR activation and repression of *lncIRF8* and *IRF8* promoters were achieved by dCAS9-VP64_GFP (Addgene #61422) (Konermann et al., 2015) and pTet-KRAB-dCas9-GFP (Xu et al., 2021), respectively.

Lentivirus infection

gRNAs, *lncIRF8*, dCas9-VP64-GFP, and KRAB-dCas9-GFP were delivered into HoxB8 MPP by lentiviral infection. Briefly, lentiviral particles were produced by calcium phosphate transfection (Graham and van der Eb, 1973) of HEK293T cells with psPAX2, pMD2.G, and the lentiviral transfer vector. At 48 and 72 hours after HEK293T cell transfection, supernatant containing virus particles was collected and concentrated using chondroitin sulfate sodium salt (CSS) and polybrene precipitation (Landázuri et al., 2007). HoxB8 MPP were infected twice with concentrated virus and subjected to Ficoll (Pancoll) purification to remove precipitate and dead cells.

Genetically modified HoxB8 MPP cell lines

***lncIRF8*-promoter KO**

Mx-Cas9-GFP HoxB8 MPP were used to generate *lncIRF8* promoter knockout (KO) HoxB8 MPP by CRISPR/Cas9. Briefly, two gRNAs for *lncIRF8*-promoter KO (Resource Table) were designed with the IDT online gRNA design tool (https://eu.idtdna.com/site/order/designtool/index/CRISPR_SEQUENCE). gRNAs were cloned into pLKO5.sgRNA.EFS.tRFP and pLKO5.sgRNA.EFS.tRFP657 vectors (Heckl et al., 2014) using BsmBI-v2, respectively.

One 10 cm dish (Bio-One) with 1.8 million HEK293T cells (70%-80% confluency) in 10 ml DMEM plus supplements (see above) was used to produce gRNA expressing lentivirus particles. HEK293T cells were transfected with 10 µg gRNA vector, 7.5 µg psPAX2, and 2.5 µg pMD2.G per gRNA by calcium phosphate transfection and lentivirus particles were harvested 48 and 72 hours after transfection.

The gRNA expressing lentiviral particles were used to infect 3 million Mx-Cas9-GFP HoxB8 MPP. Cas9 and GFP expression were induced by mIFNα (1000 IU/ml) for 4 hours, followed by FACS sorting for cells expressing the two gRNAs and Cas9 (GFP^+ RFP^+ $RFP657^+$ cells). Three thousand sorted HoxB8 MPP were then subjected to limiting dilution to obtain single-cell clones.

Single-cell colonies were genotyped by genomic PCR with primers listed in Resource Table. PCR products were sequenced by Eurofins Genomics and sequences were analyzed by SnapGene. Potential off-targets were routinely predicted by online software tools such as CRISPR-Cas9 gRNA checker (https://eu.idtdna.com/site/order/designtool/in-dex/CRISPR _SEQUENCE). Finally, 5 out of 71 single-cell colonies with homozygous deletions were subjected to off-target analysis. The top 2-5 predicted coding or non-coding targets were selected and HoxB8 MPP clones without off-target effects, or where off-target effects occurred in genes that were not expressed in MPP, CDP and DC subsets, were used for further studies (Table S1).

***lncIRF8* overexpression and *lncIRF8* knockout rescue**

lncIRF8 overexpression was performed in wild-type HoxB8 MPP. Lentiviral particles expressing *lncIRF8* were produced from ten 6 cm dishes (Bio-One), each consisting of 0.75 million HEK293T cells (70-80% confluency) in 5 ml DMEM with supplements (see above). HEK293T cells were transfected with 5 µg p*lncIRF8*-pA or pGFP-pA, 2.5 µg psPAX2, and 2.5 µg pMD2.G. Lentivirus particles were concentrated as above and used to infect 0.5 million HoxB8 MPP; single-cell clones were generated by limiting dilution and genotyped using the primers listed in Resource Table. Two out of 47 HoxB8 MPP colonies with p*lncIRF8*-pA and 3 out of 19 HoxB8 MPP colonies with pGFP-pA (control) were expanded and subjected to Flt3L-directed DC differentiation.

lncIRF8 knockout rescue was carried out in *lncIRF8*-promoter KO HoxB8 MPP. FACS sorted cells (100 cells) that genotyped as *lncIRF8*-promoter KO homozygous deletion cells, were infected with lentiviral

particles expressing *lncIRF8*. Lentiviral infection conditions were the same as for *lncIRF8* overexpression in wild-type HoxB8 MPP (see above).

CRISPR activation and CRISPR interference

CRISPR activation and CRISPR interference were performed by infecting wild-type HoxB8 MPP with lentiviral particles expressing dCAS9-VP64_GFP and pTet-KRAB-dCas9-GFP, respectively. The virus particles were produced as in the *lncIRF8* overexpression experiments. In brief, virus particles from ten 6 cm dishes were used to infect 0.5 million wild-type HoxB8 MPP, followed by FACS sorting for GFP^+ cells expressing dCas9-VP64 or dCas9-KRAB. Doxycycline (1 µg/ml) was used to induce dCas9-KRAB expression 2 days before cell sorting.

gRNAs targeting *lncIRF8* and *IRF8* promoters were cloned into pLKO5.sgRNA.EFS.tRFP as above. The dCas9-VP64-GFP and dCas9-KRAB-GFP HoxB8 MPP were then infected with specific gRNAs for gene activation and repression. The conditions for gRNA infection were the same as in *lncIRF8*-promoter KO experiments. Doxycycline (1 µg/ml) was given to the sorted dCas9-KRAB-GFP cells every 3 days to ensure sustained dCas9-KRAB expression.

Flow cytometry analysis and cell sorting

DC subsets were analyzed by flow cytometry using FACS Canto II or LSR Fortessa (both BD Biosciences). The information for flow cytometry antibodies is shown in Resource Table. For live/dead staining, cells were incubated with 3 µl 7-AAD per test for 5-10 min before flow cytometry measurement. Cells were sorted by FACS Aria IIu or FACS Melody, and flow cytometry data were analyzed by FlowJo V10 (all from BD Biosciences). Data on DC frequencies were subjected to the hierarchical clustering and represented in heatmap format using the online tool MORPHEUS (https://software.broadinstitute.org/morpheus/).

Cell transplantation

CD45.1 recipient mice were sublethal irradiated (6.0 Gy, CP-160 Faxitron) 1 day before transplantation. *lncIRF8*-promoter KO and control HoxB8 MPP (single-cell clones) were expanded *in vitro* as described above. Cells were injected into recipient mice via the tail vein (5 million cells in 100 µl PBS per mouse). Donor cells from bone marrow and spleen were subjected to flow cytometry analysis at 7 and 14 days after cell transplantation.

RT-qPCR

RNA was isolated by using the NucleoSpin RNA kit (Macherey-Nagel, 740955.250) according to the manufacturer's instructions. RNA was subjected to cDNA synthesis using the High-Capacity cDNA Reverse Transcription Kit (Applied Biosystems, 4368814) with Murine RNase Inhibitor (New England Biolabs, M0314S). RT-qPCR was performed by a StepOnePlus™ Real-Time PCR system (Applied Biosystems) with SYBR-green fluorescence (Applied Biosystems, 4385610). The primers for qPCR

were listed in Resource Table. Mouse *GAPDH* was used for normalization of *lncIRF8* and *IRF8* gene expression.

Identification of *lncIRF8*

De-novo transcript assembly of RNA-seq data was used to search for unknown transcripts with no coding potential and this identified the pDC specific lncRNA *TCONS_00190250* (referred to as *lncIRF8*) and the cDC1 specific lncRNA *TCONS_00190258*. In brief, paired end 2×100 bps reads from RNA-seq of MPP, CDP, cDC1, cDC2 and pDC were aligned to mm9 genome using Star aligner (version 2.4) (Dobin et al., 2013) and run for Cufflinks (version 2.0) (Trapnell et al., 2012). Data were subjected to lenient filtering with the parameters: min isoform fraction 0.1% and pre-RNA-fraction of 0.1%, and ribosomal genes were also filtered. Next, all the predicted transcripts were merged with cuffmerge and all transcripts with no overlap with known transcripts in mouse GENCODE were selected for further analysis (Frankish et al., 2019). The coding potential and conservation of coding elements of the lncRNAs were checked with CPAT (Wang et al., 2013) and PhyloCSF (Lin et al., 2011), respectively. *lncIRF8* (*TCONS_00190250*) and *TCONS_00190258* show low scores in both analyses, which faithfully supports their role as non-coding genes and exhibit low cross-species conservation.

To further characterize the major transcripts of *lncIRF8*, 3' and 5' end Rapid Amplification of cDNA Ends (RACE) PCR was performed using template-switching RT enzyme mix (New England Biolabs, M0466) and TA cloning kit (Thermo Fisher Scientific, K202020). The primers (listed in Resource Table) used for RACE PCR were synthesized by Eurofins Genomics except for 5' RACE-TSO, which was from IDT.

3' RACE PCR

Reverse transcript (RT) and template-switching: 4 µl (10 ng to 1 µg) total RNA (from DC differentiation day 5) were incubated at 80°C for 3 minutes and cooled rapidly on ice. RNA was then incubated with template-switching RT buffer, 1 mM dNTP, 5 mM DTT, 10 µM QT primer (Scotto-Lavino et al., 2006) and 1 µl RT enzyme in 10 µl at room temperature for 5 minutes, followed by 1 hour at 42°C, 10 minutes at 50°C, and 85°C for 5 minutes to inactive the RT enzyme mix and sample was then kept at 4°C and diluted with 20 µl MilliQ water.

First-round PCR: 1 µl of diluted sample was subjected to the first round PCR with Q0 primer and 3' RACE-GSP-*lncIRF8*-F1 (10 µM) using Q5 high fidelity DNA polymerase. Second-round PCR: the PCR products from the first round PCR (1:20 dilution) was then used as template for the second round of PCR by using Q1 primer (10 µM), 3' RACE-GSP-*lncIRF8*-F2 (10 µM). Q0 and Q1 primers and the PCR programs are described in (Scotto-Lavino et al., 2006). Products from the second-round PCR were purified using the PCR clean-up kit (Macherey-Nagel, 740609.50).

A-tailing and TA cloning: a reaction containing 5 µl of PCR clean-up product in Taq buffer, 1 mM $MgCl_2$, 0.4 mM dATP and 1 µl Taq DNA polymerase in 25 µl was prepared and incubated at 70°C for 20

minutes for A-tailing of PCR products. Five µl of the A-tailed products were subjected to TA cloning into pCR2.1 vector according to the manufacturer's instruction followed by Sanger sequencing.

5' RACE PCR

In order to identify the TSS of *lncIRF8*, template RNA from bone marrow cell-derived pDC was used to perform 5' RACE PCR using template-switching RT enzyme mix (New England Biolabs, M0466) according to the manufacturer's instructions. Template switching was by 5' RACE-GSP-*lncIRF8*-R2 primer (10 µM) and template switching oligo (TSO) (75 µM). Similar to the 3' RACE PCR, two rounds of PCR were used to improve PCR specificity. In brief, 5' RACE-GSP-*lncIRF8*-R2 (10 µM) and TSO-specific primer (10 µM) were used to perform the first-round PCR, 5' RACE-GSP-*lncIRF8*-R1 primer (10 µM) and the TSO-specific primer (10 µM) were used to perform the second round PCR, followed by fragments A-tailing, TA cloning, and Sanger sequencing as described above for 3' RACE PCR.

Identification of transcription factor binding sites

Transcription factor binding sites (TFBS) in the *IRF8* +32 kb enhancer were predicted using a motif matching tool based on the MOODS (Korhonen et al., 2009) and position weight matrixes (PWMs) were obtained from the JASPAR database (Fornes et al., 2020). The bit-score cut-off thresholds were determined by applying the dynamic programming approach as described in (Wilczynski et al., 2009) with an FPR of 0.0001. DC TF were considered and are depicted.

Statistical analysis

Statistical analyses were performed using Prism (GraphPad). Unpaired t test and Multiple t-tests were used to compare data from two groups, two-way ANOVA with Tukey's multiple comparisons test was used to analyze data from more than two groups.

References

Allhoff, M., Seré, K., Chauvistré, H., Lin, Q., Zenke, M., and Costa, I.G. (2014). Detecting differential peaks in ChIP-seq signals with ODIN. Bioinformatics *30*, 3467-3475.

Allhoff, M., Seré, K., F. Pires, J., Zenke, M., and G. Costa, I. (2016). Differential peak calling of ChIP-seq signals with replicates with THOR. Nucleic Acids Res. *44*, e153.

Alvarez-Dominguez, J.R., Bai, Z., Xu, D., Yuan, B., Lo, K.A., Yoon, M.J., Lim, Y.C., Knoll, M., Slavov, N., Chen, S., et al. (2015). De novo reconstruction of adipose tissue transcriptomes reveals long non-coding RNA regulators of brown adipocyte development. Cell Metab. *21*, 764-776.

Anderson, D.A., Dutertre, C.-A., Ginhoux, F., and Murphy, K.M. (2021). Genetic models of human and mouse dendritic cell development and function. Nature Reviews: Immunology *21*, 101-115.

Anderson III, D.A., Ou, F., Kim, S., Murphy, T.L., and Murphy, K.M. (2021). Transition from *cMyc* to *L-Myc* during dendritic cell development coordinated by rising levels of IRF8. J. Exp. Med. *219*, e20211483.

Bagadia, P., Huang, X., Liu, T.-T., Durai, V., Grajales-Reyes, G.E., Nitschké, M., Modrusan, Z., Granja, J.M., Satpathy, A.T., Briseño, C.G., et al. (2019). An *Nfil3–Zeb2–Id2* pathway imposes *Irf8* enhancer switching during cDC1 development. Nat. Immunol. *20*, 1174-1185.

Bornstein, C., Winter, D., Barnett-Itzhaki, Z., David, E., Kadri, S., Garber, M., and Amit, I. (2014). A negative feedback loop of transcription factors specifies alternative dendritic cell chromatin States. Mol. Cell *56*, 749-762.

Cabeza-Cabrerizo, M., Cardoso, A., Minutti, C.M., Pereira da Costa, M., and Reis, E.S.C. (2021). Dendritic cells revisited. Annu. Rev. Immunol *39*, 131-166.

Caviness, K., Cicchini, L., Rak, M., Umashankar, M., and Goodrum, F. (2014). Complex expression of the UL136 gene of human cytomegalovirus results in multiple protein isoforms with unique roles in replication. J. Virol. *88*, 14412-14425.

Chang, T.-H., Xu, S., Tailor, P., Kanno, T., and Ozato, K. (2012). The small ubiquitin-like modifier-deconjugating enzyme sentrin-specific peptidase 1 switches IFN regulatory factor 8 from a repressor to an activator during macrophage activation. J. Immunol. *189*, 3548-3556.

Chang, Y.K., Zuo, Z., and Stormo, G.D. (2018). Quantitative profiling of BATF family proteins/JUNB/IRF hetero-trimers using Spec-seq. BMC Mol. Biol. *19*, 1-9.

Chauvistré, H., and Seré, K. (2020). Epigenetic aspects of DC development and differentiation. Mol. Immunol. *128*, 116-124.

Corces, M.R., Trevino, A.E., Hamilton, E.G., Greenside, P.G., Sinnott-Armstrong, N.A., Vesuna, S., Satpathy, A.T., Rubin, A.J., Montine, K.S., Wu, B., et al. (2017). An improved ATAC-seq protocol reduces background and enables interrogation of frozen tissues. Nat. Methods *14*, 959-962.

Cytlak, U., Resteu, A., Pagan, S., Green, K., Milne, P., Maisuria, S., McDonald, D., Hulme, G., Filby, A., Carpenter, B., et al. (2020). Differential IRF8 transcription factor requirement defines two pathways of dendritic cell development in humans. Immunity *53*, 353-370. e358.

Dobin, A., Davis, C.A., Schlesinger, F., Drenkow, J., Zaleski, C., Jha, S., Batut, P., Chaisson, M., and Gingeras, T.R. (2013). STAR: ultrafast universal RNA-seq aligner. Bioinformatics *29*, 15-21.

Downes, D.J., Beagrie, R.A., Gosden, M.E., Telenius, J., Carpenter, S.J., Nussbaum, L., De Ornellas, S., Sergeant, M., Eijsbouts, C.Q., Schwessinger, R., et al. (2021). High-resolution targeted 3C interrogation of cis-regulatory element organization at genome-wide scale. Nat. Commun. *12*, 531.

Downes, D.J., Smith, A.L., Karpinska, M.A., Velychko, T., Rue-Albrecht, K., Sims, D., Milne, T.A., Davies, J.O., Oudelaar, A.M., and Hughes, J.R. (2022). Capture-C: a modular and flexible approach for high-resolution chromosome conformation capture. Nat. Protoc. *17*, 445-475.

Dress, R.J., Dutertre, C.-A., Giladi, A., Schlitzer, A., Low, I., Shadan, N.B., Tay, A., Lum, J., Kairi, M.F.B.M., Hwang, Y.Y., et al. (2019). Plasmacytoid dendritic cells develop from Ly6D+ lymphoid progenitors distinct from the myeloid lineage. Nat. Immunol. *20*, 852-864.

Durai, V., Bagadia, P., Granja, J.M., Satpathy, A.T., Kulkarni, D.H., Davidson, J.T., Wu, R., Patel, S.J., Iwata, A., Liu, T.-T., et al. (2019). Cryptic activation of an *Irf8* enhancer governs cDC1 fate specification. Nat. Immunol. *20*, 1161-1173.

Felker, P., Seré, K., Lin, Q., Becker, C., Hristov, M., Hieronymus, T., and Zenke, M. (2010). TGF-β1 accelerates dendritic cell differentiation from common dendritic cell progenitors and directs subset

specification toward conventional dendritic cells. J. Immunol. *185*, 5326-5335.

Fischer, M., Goldschmitt, J., Peschel, C., Brakenhoff, J.P., Kallen, K.-J., Wollmer, A., Grötzinger, J., and Rose-John, S. (1997). A bioactive designer cytokine for human hematopoietic progenitor cell expansion. Nat. Biotechnol. *15*, 142-145.

Fornes, O., Castro-Mondragon, J.A., Khan, A., Van der Lee, R., Zhang, X., Richmond, P.A., Modi, B.P., Correard, S., Gheorghe, M., Baranašić, D., et al. (2020). JASPAR 2020: update of the open-access database of transcription factor binding profiles. Nucleic Acids Res. *48*, D87-D92.

Frankish, A., Diekhans, M., Ferreira, A.-M., Johnson, R., Jungreis, I., Loveland, J., Mudge, J.M., Sisu, C., Wright, J., Armstrong, J., et al. (2019). GENCODE reference annotation for the human and mouse genomes. Nucleic Acids Res. *47*, D766-D773.

Garber, M., Yosef, N., Goren, A., Raychowdhury, R., Thielke, A., Guttman, M., Robinson, J., Minie, B., Chevrier, N., Itzhaki, Z., et al. (2012). A high-throughput chromatin immunoprecipitation approach reveals principles of dynamic gene regulation in mammals. Mol. Cell *47*, 810-822.

Gibson, D.G., Young, L., Chuang, R.-Y., Venter, J.C., Hutchison, C.A., and Smith, H.O. (2009). Enzymatic assembly of DNA molecules up to several hundred kilobases. Nat. Methods *6*, 343-345.

Graf, T., and Enver, T. (2009). Forcing cells to change lineages. Nature *462*, 587-594.

Graham, F.L., and van der Eb, A.J. (1973). A new technique for the assay of infectivity of human adenovirus 5 DNA. Virology *52*, 456-467.

Grajales-Reyes, G.E., Iwata, A., Albring, J., Wu, X., Tussiwand, R., Wumesh, K., Kretzer, N.M., Briseño, C.G., Durai, V., Bagadia, P., et al. (2015). Batf3 maintains autoactivation of *Irf8* for commitment of a CD8α+ conventional DC clonogenic progenitor. Nat. Immunol. *16*, 708-717.

Heckl, D., Kowalczyk, M.S., Yudovich, D., Belizaire, R., Puram, R.V., McConkey, M.E., Thielke, A., Aster, J.C., Regev, A., and Ebert, B.L. (2014). Generation of mouse models of myeloid malignancy with combinatorial genetic lesions using CRISPR-Cas9 genome editing. Nat. Biotechnol. *32*, 941-946.

Huang, X., Nandakumar, V., Tumurkhuu, G., Wang, T., Hong, B., Jones, L., Won, H., Yoshii, H., Ozato, K., Masumi, A., et al. (2016). Mysm1 is required for interferon regulatory factor expression in maintaining HSC quiescence and thymocyte development. Cell Death Dis. *7*, e2260-e2260.

Humblin, E., Thibaudin, M., Chalmin, F., Derangère, V., Limagne, E., Richard, C., Flavell, R.A., Chevrier, S., Ladoire, S., Berger, H., et al. (2017). IRF8-dependent molecular complexes control the Th9 transcriptional program. Nat. Commun. *8*, 2085.

Konermann, S., Brigham, M.D., Trevino, A.E., Joung, J., Abudayyeh, O.O., Barcena, C., Hsu, P.D., Habib, N., Gootenberg, J.S., Nishimasu, H., et al. (2015). Genome-scale transcriptional activation by an engineered CRISPR-Cas9 complex. Nature *517*, 583-588.

Konieczna, I., Horvath, E., Wang, H., Lindsey, S., Saberwal, G., Bei, L., Huang, W., Platanias, L., and Eklund, E.A. (2008). Constitutive activation of SHP2 in mice cooperates with ICSBP deficiency to accelerate progression to acute myeloid leukemia. J. Clin. Invest. *118*, 853-867.

Korhonen, J., Martinmäki, P., Pizzi, C., Rastas, P., and Ukkonen, E. (2009). MOODS: fast search for position weight matrix matches in DNA sequences. Bioinformatics *25*, 3181-3182.

Kühn, R., Schwenk, F., Aguet, M., and Rajewsky, K. (1995). Inducible gene targeting in mice. Science *269*, 1427-1429.

Kurotaki, D., Kawase, W., Sasaki, H., Nakabayashi, J., Nishiyama, A., Morse III, H.C., Ozato, K., Suzuki, Y., and Tamura, T. (2019). Epigenetic control of early dendritic cell lineage specification by the transcription factor IRF8 in mice. Blood *133*, 1803-1813.

Kurotaki, D., Yamamoto, M., Nishiyama, A., Uno, K., Ban, T., Ichino, M., Sasaki, H., Matsunaga, S., Yoshinari, M., Ryo, A., et al. (2014). IRF8 inhibits C/EBPα activity to restrain mononuclear phagocyte progenitors from differentiating into neutrophils. Nat. Commun. *5*, 4978.

Landázuri, N., Krishna, D., Gupta, M., and Doux, J.M.L. (2007). Retrovirus-polymer complexes: study of the factors affecting the dose response of transduction. Biotechnol. Prog. *23*, 480-487.

Langmead, B., and Salzberg, S.L. (2012). Fast gapped-read alignment with Bowtie 2. Nat. Methods *9*, 357-359.

Lau, C.M., Tiniakou, I., Perez, O.A., Kirkling, M.E., Yap, G.S., Hock, H., and Reizis, B. (2018). Transcription factor Etv6 regulates functional differentiation of cross-presenting classical dendritic cells. J. Exp. Med. *215*, 2265-2278.

Laurenti, E., and Göttgens, B. (2018). From haematopoietic stem cells to complex differentiation landscapes. Nature *553*, 418-426.

Li, Z., Schulz, M.H., Look, T., Begemann, M., Zenke, M., and Costa, I.G. (2019). Identification of transcription factor binding sites using ATAC-seq. Genome Biol. *20*, 1-21.

Lin, M.F., Jungreis, I., and Kellis, M. (2011). PhyloCSF: a comparative genomics method to distinguish protein coding and non-coding regions. Bioinformatics *27*, i275-i282.

Lin, Q., Chauvistré, H., Costa, I.G., Gusmao, E.G., Mitzka, S., Hänzelmann, S., Baying, B., Klisch, T., Moriggl, R., Hennuy, B., et al. (2015). Epigenetic program and transcription factor circuitry of dendritic cell development. Nucleic Acids Res. *43*, 9680-9693.

Loughran, S.J., Haas, S., Wilkinson, A.C., Klein, A.M., and Brand, M. (2020). Lineage commitment of hematopoietic stem cells and progenitors: insights from recent single cell and lineage tracing technologies. Exp. Hematol. *88*, 1-6.

Manguso, R.T., Pope, H.W., Zimmer, M.D., Brown, F.D., Yates, K.B., Miller, B.C., Collins, N.B., Bi, K., LaFleur, M.W., Juneja, V.R., et al. (2017). In vivo CRISPR screening identifies Ptpn2 as a cancer immunotherapy target. Nature *547*, 413-418.

Misteli, T., and Finn, E.H. (2021). Chromatin architecture is a flexible foundation for gene expression. Nat. Genet. *53*, 426-427.

Murakami, K., Sasaki, H., Nishiyama, A., Kurotaki, D., Kawase, W., Ban, T., Nakabayashi, J., Kanzaki, S., Sekita, Y., Nakajima, H., et al. (2021). A RUNX–CBFβ-driven enhancer directs the *Irf8* dose-dependent lineage choice between DCs and monocytes. Nat. Immunol. *22*, 301-311.

Nishimura, S., Takahashi, S., Kuroha, T., Suwabe, N., Nagasawa, T., Trainor, C., and Yamamoto, M. (2000). A GATA box in the GATA-1 gene hematopoietic enhancer is a critical element in the network of GATA factors and sites that regulate this gene. Mol. Cell. Biol. *20*, 713-723.

Nutt, S.L., and Chopin, M. (2020). Transcriptional networks driving dendritic cell differentiation and function. Immunity *52*, 942-956.

Okuno, Y., Huang, G., Rosenbauer, F., Evans, E.K., Radomska, H.S., Iwasaki, H., Akashi, K., Moreau-Gachelin, F., Li, Y., Zhang, P., et al. (2005). Potential autoregulation of transcription factor PU. 1 by an upstream regulatory element. Mol. Cell. Biol. *25*, 2832-2845.

Oudelaar, A.M., Beagrie, R.A., Gosden, M., de Ornellas, S., Georgiades, E., Kerry, J., Hidalgo, D., Carrelha, J., Shivalingam, A., El-Sagheer, A.H., et al. (2020). Dynamics of the 4D genome during in vivo lineage specification and differentiation. Nat. Commun. *11*, 2722.

Oudelaar, A.M., and Higgs, D.R. (2021). The relationship between genome structure and function. Nature Reviews: Genetics *22*, 154-168.

Owens, D.D., Anselmi, G., Oudelaar, A.M., Downes, D.J., Cavallo, A., Harman, J.R., Schwessinger, R., Bucakci, A., Greder, L., de Ornellas, S., et al. (2022). Dynamic Runx1 chromatin boundaries affect gene expression in hematopoietic development. Nat. Commun. *13*, 773.

Platt, R.J., Chen, S., Zhou, Y., Yim, M.J., Swiech, L., Kempton, H.R., Dahlman, J.E., Parnas, O., Eisenhaure, T.M., Jovanovic, M., et al. (2014). CRISPR-Cas9 knockin mice for genome editing and cancer modeling. Cell *159*, 440-455.

Redecke, V., Wu, R., Zhou, J., Finkelstein, D., Chaturvedi, V., High, A.A., and Häcker, H. (2013). Hematopoietic progenitor cell lines with myeloid and lymphoid potential. Nat. Methods *10*, 795-803.

Rodrigues, P.F., Alberti-Servera, L., Eremin, A., Grajales-Reyes, G.E., Ivanek, R., and Tussiwand, R. (2018). Distinct progenitor lineages contribute to the heterogeneity of plasmacytoid dendritic cells. Nat. Immunol. *19*, 711-722.

Rodrigues, P.F., and Tussiwand, R. (2020). Novel concepts in plasmacytoid dendritic cell (pDC) development and differentiation. Mol. Immunol. *126*, 25-30.

Sanborn, A.L., Rao, S.S., Huang, S.-C., Durand, N.C., Huntley, M.H., Jewett, A.I., Bochkov, I.D., Chinnappan, D., Cutkosky, A., Li, J., et al. (2015). Chromatin extrusion explains key features of loop and domain formation in wild-type and engineered genomes. Proc. Natl. Acad. Sci. USA *112*, E6456-E6465.

Sartorelli, V., and Lauberth, S.M. (2020). Enhancer RNAs are an important regulatory layer of the epigenome. Nat. Struct. Mol. Biol. *27*, 521-528.

Schiavoni, G., Mattei, F., Sestili, P., Borghi, P., Venditti, M., Morse III, H.C., Belardelli, F., and Gabriele,

L. (2002). ICSBP is essential for the development of mouse type I interferon-producing cells and for the generation and activation of CD8α+ dendritic cells. J. Exp. Med. *196*, 1415-1425.

Schönheit, J., Kuhl, C., Gebhardt, M.L., Klett, F.F., Riemke, P., Scheller, M., Huang, G., Naumann, R., Leutz, A., Stocking, C., et al. (2013). PU. 1 level-directed chromatin structure remodeling at the Irf8 gene drives dendritic cell commitment. Cell Rep. *3*, 1617-1628.

Scotto-Lavino, E., Du, G., and Frohman, M.A. (2006). 3' end cDNA amplification using classic RACE. Nat. Protoc. *1*, 2742-2745.

Sichien, D., Scott, C.L., Martens, L., Vanderkerken, M., Van Gassen, S., Plantinga, M., Joeris, T., De Prijck, S., Vanhoutte, L., Vanheerswynghels, M., et al. (2016). IRF8 transcription factor controls survival and function of terminally differentiated conventional and plasmacytoid dendritic cells, respectively. Immunity *45*, 626-640.

Stadhouders, R., Filion, G.J., and Graf, T. (2019). Transcription factors and 3D genome conformation in cell-fate decisions. Nature *569*, 345-354.

Statello, L., Guo, C.-J., Chen, L.-L., and Huarte, M. (2021). Gene regulation by long non-coding RNAs and its biological functions. Nature Reviews: Molecular Cell Biology *22*, 96-118.

Tamura, T., Kurotaki, D., and Koizumi, S.-i. (2015). Regulation of myelopoiesis by the transcription factor IRF8. Int. J. Hematol. *101*, 342-351.

Theilgaard-Mönch, K., Pundhir, S., Reckzeh, K., Su, J., Tapia, M., Furtwängler, B., Jendholm, J., Jakobsen, J.S., Hasemann, M.S., Knudsen, K.J., et al. (2022). Transcription factor-driven coordination of cell cycle exit and lineage-specification in vivo during granulocytic differentiation. Nat. Commun. *13*, 3595.

Trapnell, C., Roberts, A., Goff, L., Pertea, G., Kim, D., Kelley, D.R., Pimentel, H., Salzberg, S.L., Rinn, J.L., and Pachter, L. (2012). Differential gene and transcript expression analysis of RNA-seq experiments with TopHat and Cufflinks. Nat. Protoc. *7*, 562-578.

Tsujimura, H., Tamura, T., and Ozato, K. (2003). Cutting edge: IFN consensus sequence binding protein/IFN regulatory factor 8 drives the development of type I IFN-producing plasmacytoid dendritic cells. J. Immunol. *170*, 1131-1135.

Verlander, Z., Cummings, A., Brown, H.M., and Sen, R. (2022). Advances in understanding epigenetic impacts on dendritic cell regulation and function. Clinical and Translational Discovery *2*, e53.

Wang, L., Park, H.J., Dasari, S., Wang, S., Kocher, J.-P., and Li, W. (2013). CPAT: Coding-Potential Assessment Tool using an alignment-free logistic regression model. Nucleic Acids Res. *41*, e74.

Wilczynski, B., Dojer, N., Patelak, M., and Tiuryn, J. (2009). Finding evolutionarily conserved cis-regulatory modules with a universal set of motifs. BMC Bioinformatics *10*, 82.

Xu, H., Look, T., Prithiviraj, S., Lennartz, D., Cáceres, M.D., Götz, K., Wanek, P., Häcker, H., Kramann, R., Seré, K., et al. (2021). CRISPR/Cas9 editing in conditionally immortalized HoxB8 cells for studying gene regulation in mouse dendritic cells. Eur. J. Immunol. doi: 10.1002/eji.202149482.

Yoon, J., Feng, X., Kim, Y.-S., Shin, D.-M., Hatzi, K., Wang, H., and Morse, H.C. (2014). Interferon regulatory factor 8 (IRF8) interacts with the B cell lymphoma 6 (BCL6) corepressor BCOR. J. Biol. Chem. *289*, 34250-34257.

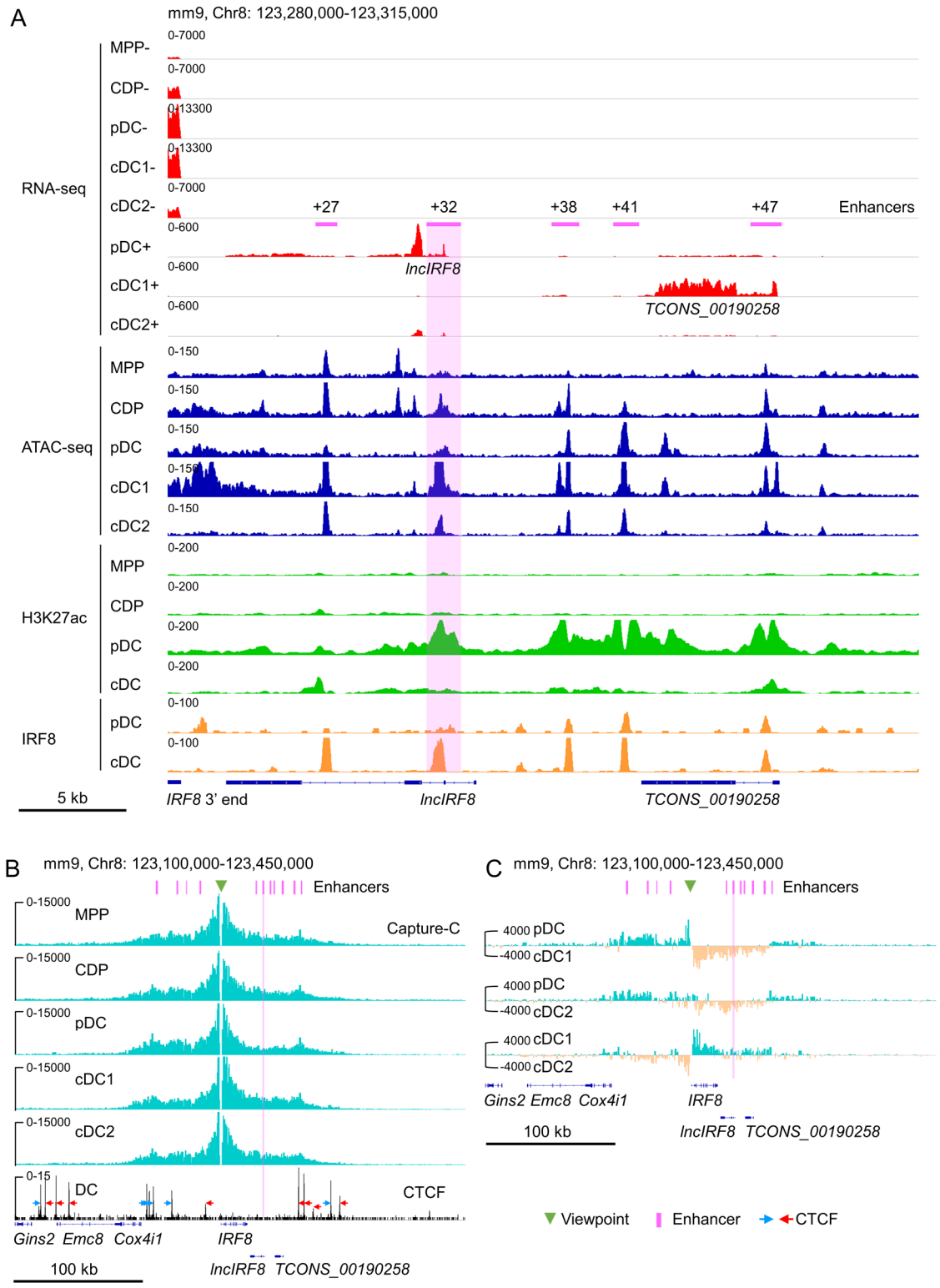

Figure 1. *IRF8* epigenetic signatures and promoter-enhancer interaction maps during DC differentiation

(A) Gene expression and epigenetic signatures of *IRF8* downstream region in MPP, CDP, pDC, all cDC, cDC1 and cDC2 are visualized by IGV browser. Gene expression was measured by RNA-seq, chromatin accessibility by ATAC-seq, H3K27ac and IRF8 binding by ChIP-seq. Positions of *IRF8* 3' end, *IRF8* enhancers, pDC specific *lncIRF8* and cDC1 specific *TCONS_00190258* lncRNA are indicated. For RNA-seq - and + strands are shown. Scale bar: 5 kb.

(B) Physical interactions of *IRF8* promoter with flanking sequences in MPP, CDP, pDC, cDC1 and cDC2 by nuclear-titrated (NuTi) Capture-C (turquoise), and CTCF binding by ChIP-seq in DC (Garber et al., 2012). Mean numbers of unique interactions normalized to a 300 kb region around the *IRF8* promoter viewpoint (green triangle) and scaled by a factor of 1,000,000 are shown (n=2). The orientations of CTCF binding are indicated with blue and red arrows. *TCONS_00190258* refers to the cDC1 specific lncRNA shown in (A). Scale bar: 100 kb.

(C) Comparations of the chromatin interactions with *IRF8* promoter in pDC, cDC1 and cDC2. Differential tracks were created by subtraction of the mean normalized tracks of (B). Pairwise comparisons are shown and color coded. Turquoise and orange tracks represent specific interactions with the *IRF8* promoter in the indicated cell types. Scale bar: 100 kb.

Purple bars and lines indicate the position of flanking enhancers relative to *IRF8* TSS. The purple bars from left to right represent -50 kb, -34 kb, -26 kb, -16 kb, +27 kb, +32 kb, +38 kb, +41 kb, +47 kb, +56 kb and +62 kb enhancer, respectively (panels B and C). *IRF8* +32 kb enhancer is highlighted by purple box.

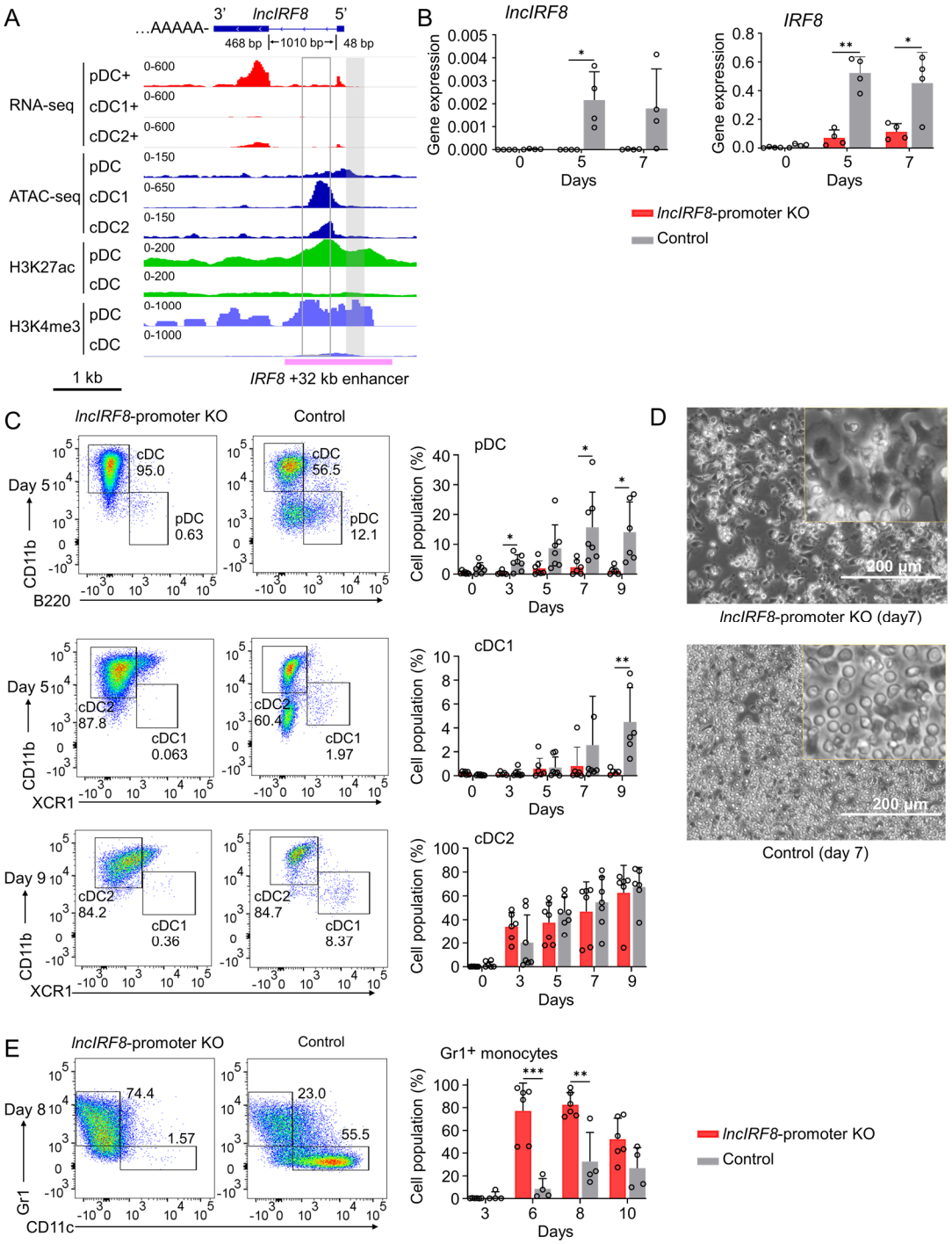

Figure 2. *lncIRF8* promoter KO compromises pDC and cDC1 development *in vitro*

(A) Genomic anatomy of *lncIRF8* locus determined by 3' and 5' RACE PCR. Blue box, exon 2 and 3 (48 bp and 468 bp, respectively). The 1010 bp intron and polyA tail are shown. Data of RNA-seq, ATAC-seq, ChIP-seq of H3K27ac (enhancer mark) and H3K4me3 (active promoter mark, near TSS) are visualized by IGV browser for the indicated cell populations (pDC, all cDC, cDC1 and cDC2). Grey box, *lncIRF8* promoter KO region; open box, cDC1 specific +32 kb enhancer by (Durai et al., 2019). *IRF8* +32 kb enhancer based on the H3K27ac enhancer mark is indicated with a purple line. Scale bar: 1 kb.

(B) Gene expression of *lncIRF8* and *IRF8* in *lncIRF8*-promoter KO and control at day 0, 5, and 7 of Flt3L directed DC differentiation. Gene expression was determined by RT-qPCR and normalized to *GAPDH*. n=4.

(C) Representative flow cytometry analysis of Flt3L directed DC differentiation of *lncIRF8*-promoter KO HoxB8 MPP and control (Xu et al., 2021). pDC, all cDC, cDC1 and cDC2 were gated as in Figure S3E and are shown. Bar diagrams depict quantification of pDC, cDC1 and cDC2 normalized to living single cells on DC differentiation day 0, 3, 5, 7 and 9. n=6-7.

(D) Representative phase-contrast microscopy images of *lncIRF8*-promoter KO HoxB8 MPP and control on day 7 of Flt3L directed DC differentiation. Scale bar: 200 µm.

(E) Representative flow cytometry analysis of spontaneous DC differentiation of *lncIRF8*-promoter KO HoxB8 MPP and control with growth factors but without E2 (Xu et al., 2021) at day 8. $Gr1^+$ monocytes and $CD11c^+$ DC are shown. Quantification of $Gr1^+$ monocytes of living single cells on day 3, 6, 8 and 10 of spontaneous DC differentiation. n=6, *lncIRF8*-promoter KO; n=4, control.

Empty gRNA vector or non-targeting gRNA vector HoxB8 MPP were used as controls. Data represent mean ± SD of at least 3 independent experiments with different HoxB8 MPP clones of *lncIRF8*-promoter KO and control without deletion. **P*<0.05, ***P*<0.01, ****P*<0.001, *****P*<0.0001, multiple t-tests. Data that have no difference (*P*>0.05) are not labeled.

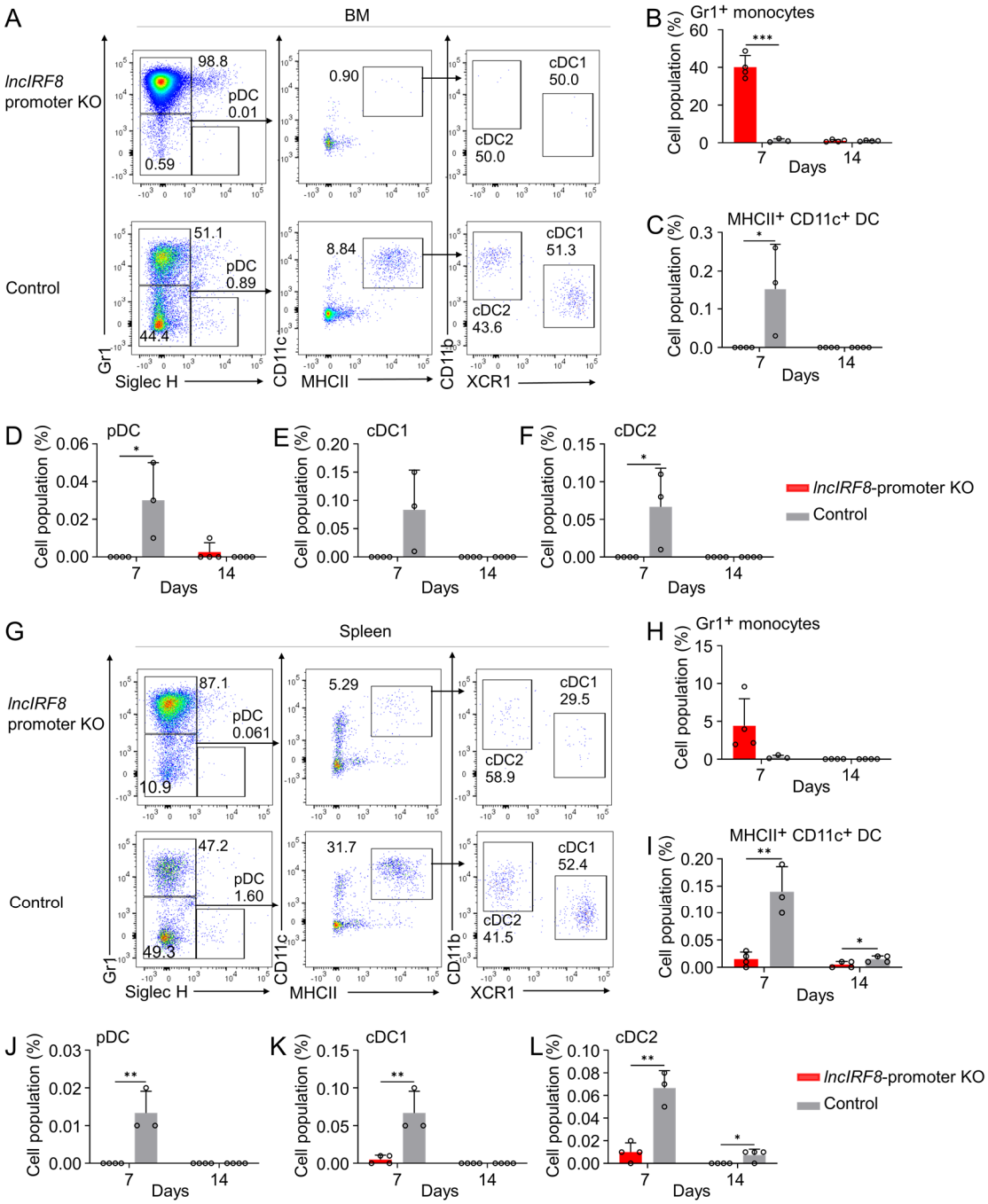

Figure 3. *lncIRF8* promoter KO comprises pDC and cDC1 development *in vivo* upon cell transplantation

(A) Representative flow cytometry analysis of CD45.2$^+$ *lncIRF8*-promoter KO and control HoxB8 MPP in BM at day 7 after cell transplantation (for details see Figure S5J and K). Donor cell populations were gated from 7-AAD$^-$ CD45.2$^+$ Lin$^-$ cells and Gr1$^+$ monocytes, pDC, cDC1 and cDC2 are shown.

(B-F) Quantification of Gr1$^+$ monocytes, MHCII$^+$ CD11c$^+$ DC, pDC, cDC1 and cDC2 of living single cells in BM on day 7 and 14 after cell transplantation (n=3-4).

(G) Representative flow cytometry analysis of *lncIRF8*-promoter KO and control HoxB8 MPP in spleen at day 7 after cell transplantation. Gating was as in panel (A).

(H-L) Quantification of Gr1$^+$ monocytes, MHCII$^+$ CD11c$^+$ DC, pDC, cDC1 and cDC2 on day 7 and 14 after cell transplantation (n=3-4).

Data represent mean ± SD from 3-4 mice. **P*<0.05, ***P*<0.01, ****P*<0.001, multiple t-tests. Data that have no difference (*P*>0.05) are not labeled.

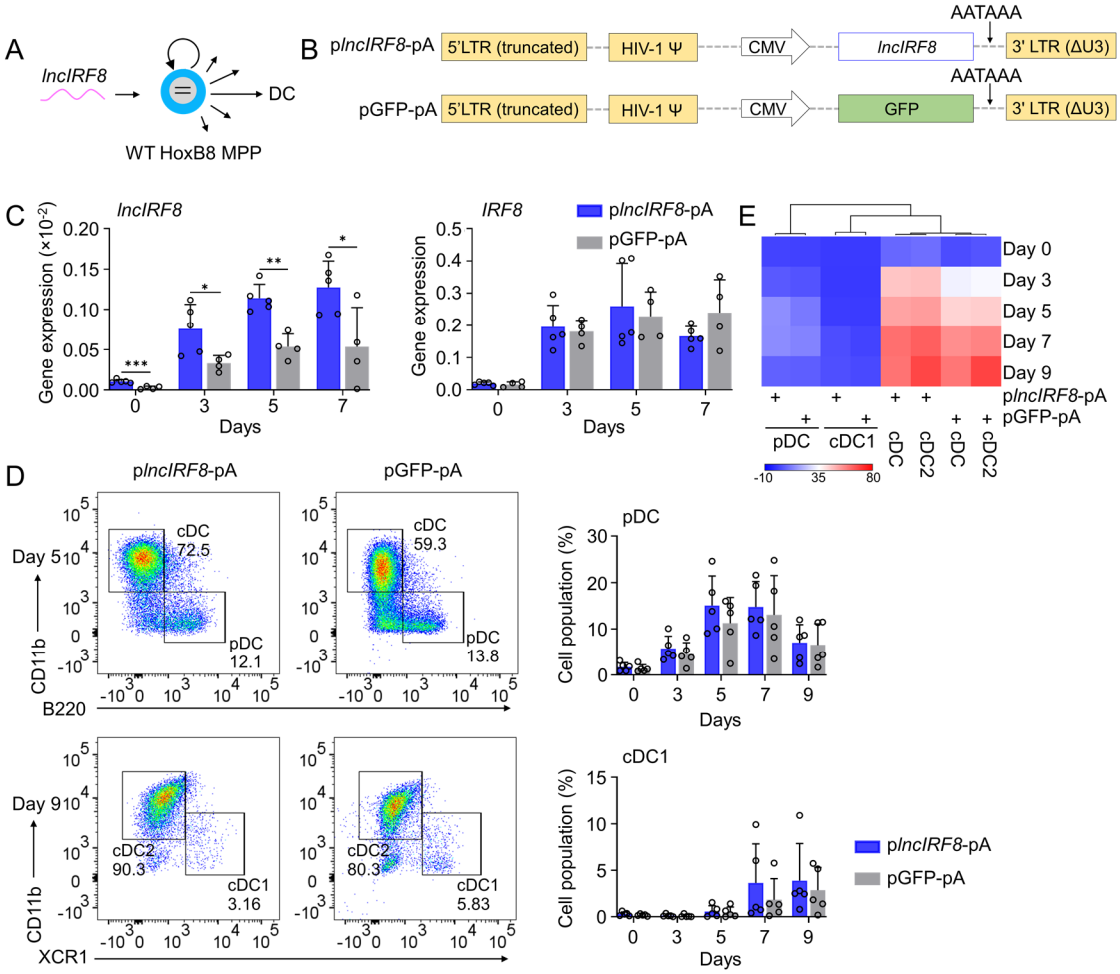

Figure 4. *lncIRF8* overexpression leaves pDC and cDC1 development unaffected

(A and B) Schematic representation of *lncIRF8* overexpression in WT HoxB8 MPP and of p*lncIRF8*-pA (*lncIRF8* overexpression) and pGFP-pA (control) plasmids. A polyA signal AATAAA for transcription termination was inserted at the 3' end of *lncIRF8* and GFP.

(C) Gene expression of *lncIRF8* and *IRF8* in p*lncIRF8*-pA and pGFP-pA HoxB8 MPP on day 0, 3, 5, and 7 of Flt3L directed DC differentiation (n=4-5). Gene expression was by RT-qPCR and normalized to *GAPDH*.

(D) Representative flow cytometry of DC subsets at day 5 and 9 of Flt3L directed DC differentiation of p*lncIRF8*-pA and pGFP-pA HoxB8 MPP. Quantification of pDC and cDC1 of living single cells on Flt3L directed DC differentiation day 0, 3, 5, 7, and 9 (n=5) is shown. Gating for pDC and cDC1 was as in Figure S3E.

(E) Heatmap representation of DC subsets of panel (D) at day 0, 3, 5, 7, and 9 of DC differentiation. Red, high frequency; white, intermediate frequency and blue, low frequency.

Data represent mean ± SD of at least 3 independent experiments with different HoxB8 MPP clones of p*lncIRF8*-pA and pGFP-pA. **P*<0.05, ***P*<0.01, ****P*<0.001, multiple t-tests. Data that have no difference (*P*>0.05) are not labeled.

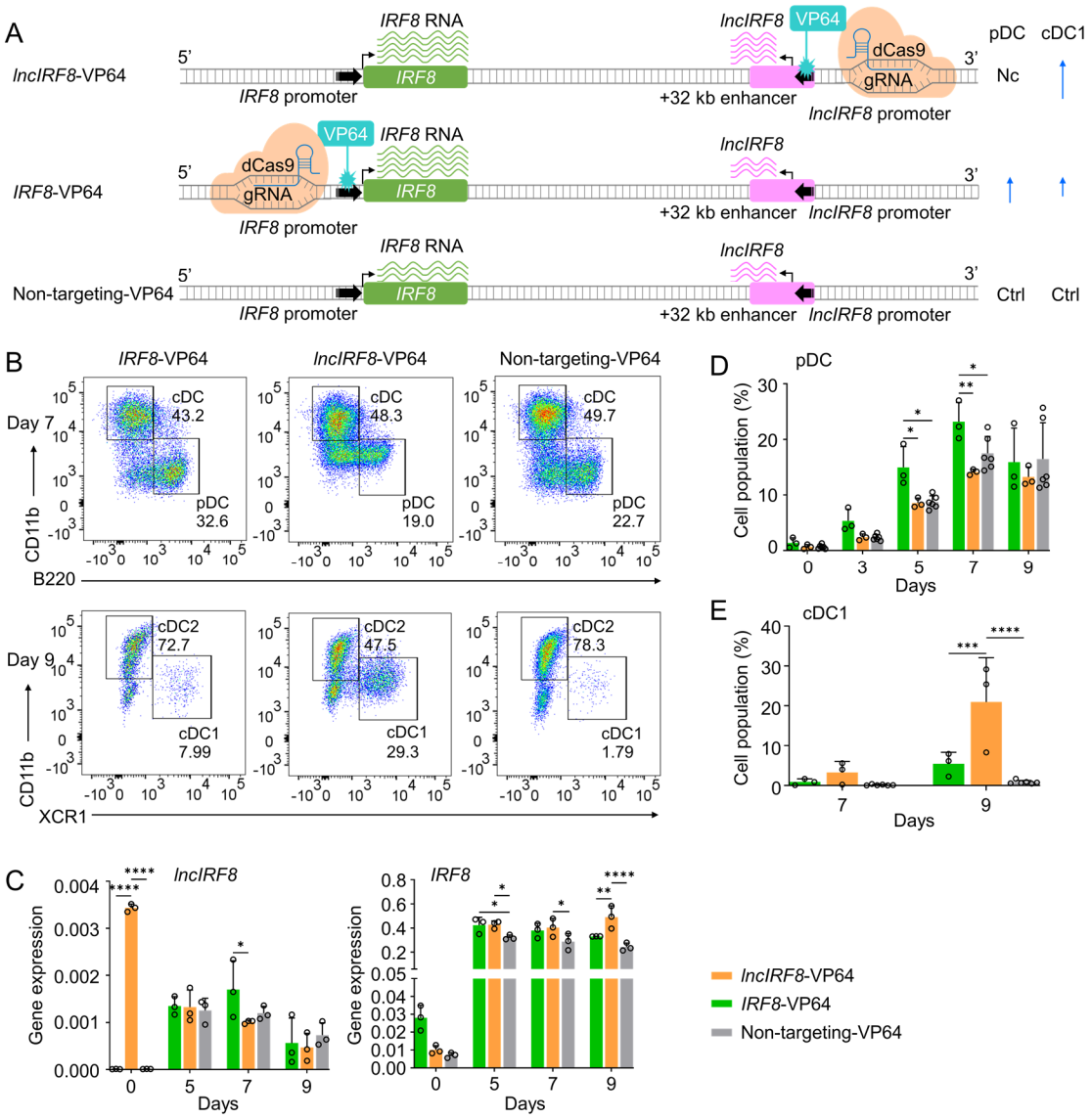

Figure 5. Activation of *lncIRF8* promoter promotes cDC1 development

(A) Schematic representation of *lncIRF8* and *IRF8* promoter activation (top and middle, respectively) by CRISPR activation with dCas9-VP64. gRNAs were positioned upstream of *lncIRF8* and *IRF8* TSS for gene activation. dCas9-VP64 cells with non-targeting gRNA were used as control (bottom). Green and purple wavy lines represent *IRF8* and *lncIRF8* RNA, respectively. The number of wavy lines indicates levels of gene transcription determined by RT-qPCR in (C). Different length of blue arrows represents the frequencies of pDC and cDC1 according to panel B, D and E. Nc, No change; Ctrl, Control.

(B) Representative flow cytometry analysis of CRISPR activation targeting the *lncIRF8* and *IRF8* promoters at day 7 and 9 of Flt3L directed DC differentiation. Two non-targeting gRNAs were used as controls and one representative non-targeting gRNA is shown (Non-targeting-VP64). Top row, $CD11b^{+}$ $B220^{-}$ cDC and $CD11b^{-}$ $B220^{+}$ pDC at day 7 of Flt3L directed DC differentiation; bottom row, $CD11b^{low/-}$ $XCR1^{+}$ cDC1 and $CD11b^{+}$ $XCR1^{-}$ cDC2 at day 9 of DC differentiation. For gating strategy see Figure S7B.

(C) Gene expression of *lncIRF8* and *IRF8* in *lncIRF8*-VP64, *IRF8*-VP64 and non-targeting-VP64 HoxB8 MPP on day 0, 5, 7, and 9 of Flt3L directed DC differentiation (n=3). Gene expression analysis was by RT-qPCR and data are normalized to *GAPDH.* Data represent mean ± SD of 3 independent experiments. **P*<0.05, ***P*<0.01, *****P*<0.0001, two-way ANOVA, Tukey's multiple comparisons test. Data that have no difference (*P*>0.05) are not labeled.

(D and E) Quantification of pDC and cDC1 in percent of living single cells as in panel (B) on various days of Flt3L directed DC differentiation (n=3). Non-targeting-VP64 refers to both non-targeting-VP64 controls (n=6). Data represent mean ± SD of 3 independent experiments. **P*<0.05, ***P*<0.01, ****P*<0.001, *****P*<0.0001, two-way ANOVA, Tukey's multiple comparisons test. Data that have no difference (*P*>0.05) are not labeled.

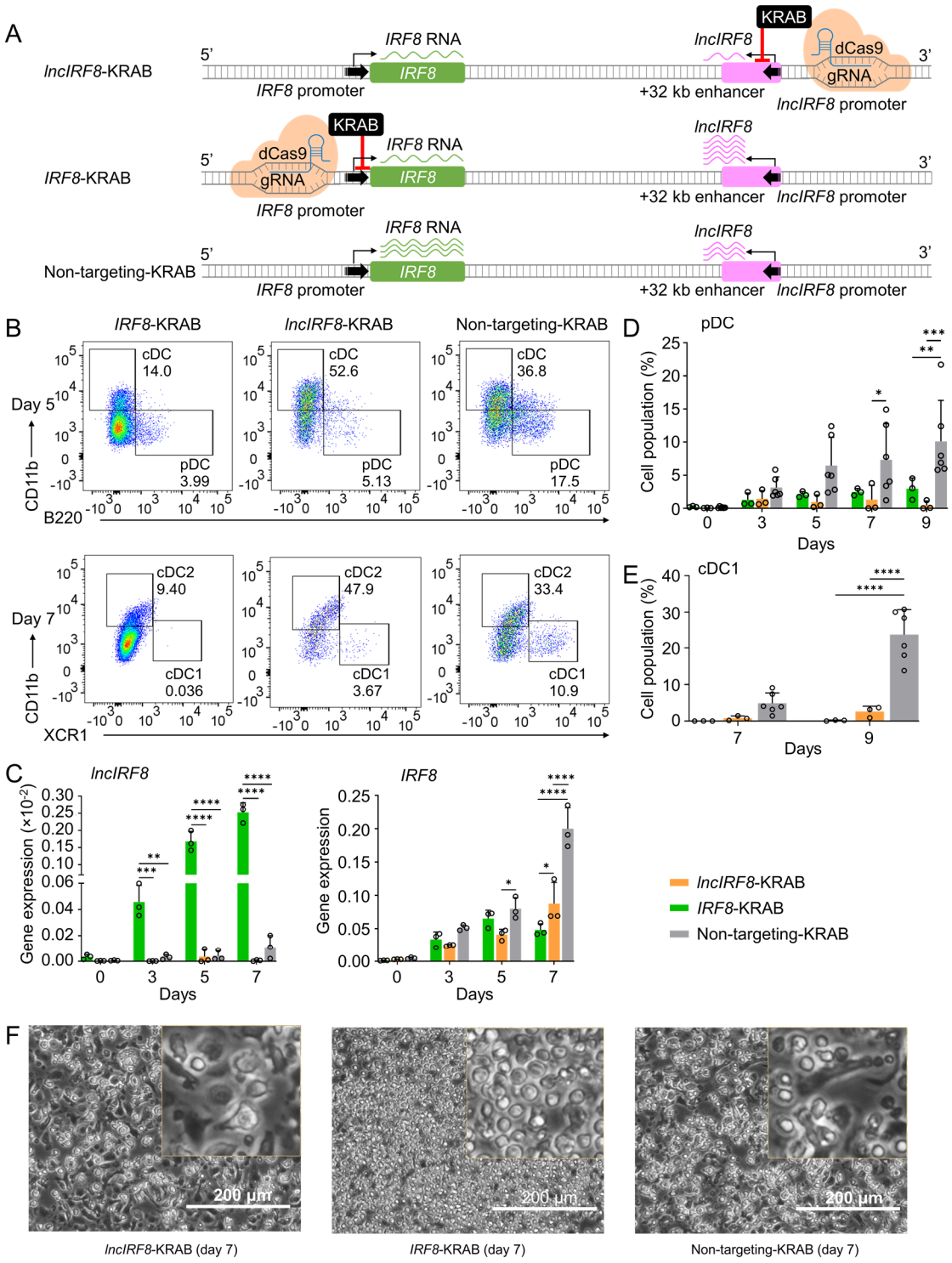

Figure 6. Repression of *lncIRF8* promoter compromises pDC and cDC1 development

(A) Schematic representation of *lncIRF8* and *IRF8* promoter repression (top and middle, respectively) by CRISPR interference with dCas9-KRAB. gRNAs were positioned downstream of *lncIRF8* and *IRF8* TSS to block gene transcription. dCas9-KRAB cells with non-targeting gRNA were used as control (bottom). Green and purple wavy lines represent *IRF8* and *lncIRF8* RNA, respectively. The number of wavy lines indicates levels of gene transcription determined by RT-qPCR in (C).

(B) Representative flow cytometry analysis of CRISPR interference targeting the *lncIRF8* and *IRF8* promoters at day 5 and 7 of Flt3L directed DC differentiation. Two non-targeting gRNAs were used as controls and one representative non-targeting gRNA is shown (Non-targeting-KRAB). cDC and pDC at day 5 and cDC1 and cDC2 at day 7 of Flt3L directed DC differentiation are shown similar to Figure 5B.

(C) Gene expression of *lncIRF8* and *IRF8* in *lncIRF8*-KRAB, *IRF8*-KRAB and non-targeting-KRAB HoxB8 MPP on day 0, 3, 5, and 7 of Flt3L directed DC differentiation (n=3). Gene expression analysis was by RT-qPCR and data are normalized to *GAPDH*. Data represent mean ± SD of 3 independent experiments. **P*<0.05, ***P*<0.01, ****P*<0.001, *****P*<0.0001, two-way ANOVA, Tukey's multiple comparisons test. Data that have no difference (*P*>0.05) are not labeled.

(D and E) Quantification of pDC and cDC1 in percent of living single cells as in panel (B) on various days of Flt3L directed DC differentiation (n=3). Non-targeting-KRAB refers to both non-targeting-KRAB controls (n=6). Data represent mean ± SD of 3 independent experiments. **P*<0.05, ***P*<0.01, ****P*<0.001, *****P*<0.0001, two-way ANOVA, Tukey's multiple comparisons test. Data that have no difference (*P*>0.05) are not labeled.

(F) Representative phase-contrast microscopy image of *lncIRF8*-KRAB, *IRF8*-KRAB and non-targeting-KRAB on day 7 of Flt3L directed DC differentiation. Scale bar: 200 µm.

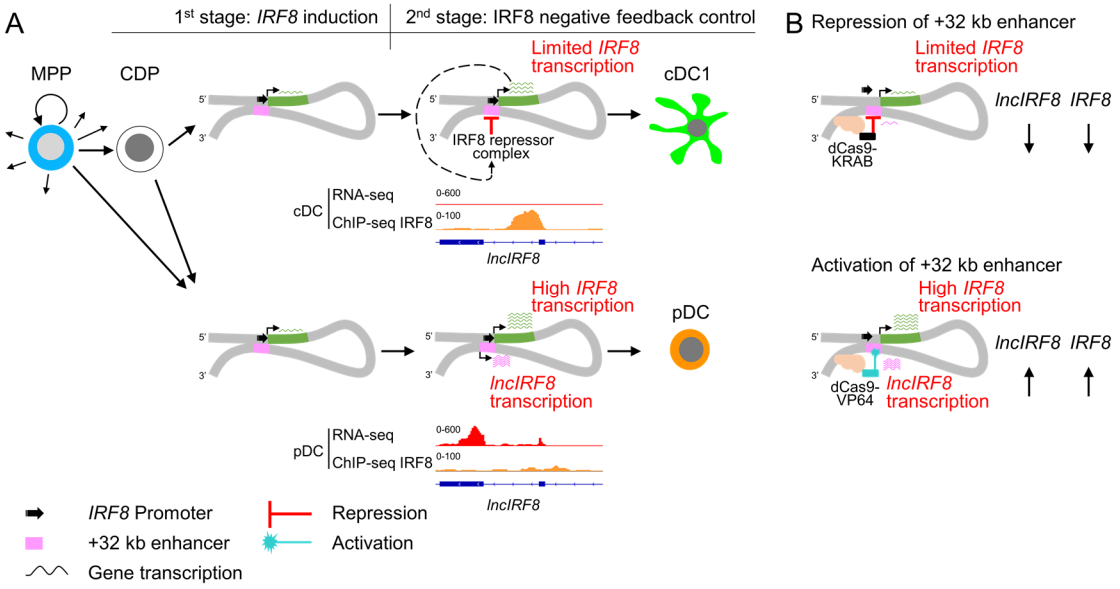

Figure 7. Negative feedback loop of *IRF8* through +32 kb enhancer governs DC differentiation

(A) Schematic representation of *IRF8* gene regulation during DC differentiation. *IRF8* transcription is induced at the CDP stage by its flanking enhancers, including the +32 kb enhancer, and is further increased in pDC and cDC1 (green wavy lines; the number of wavy lines indicates levels of gene transcription as in Figure 5A and Figure 6A). In pDC the +32 kb enhancer marked by *lncIRF8* is less repressed by IRF8 repressor complex compared to cDC1, resulting in particularly high *IRF8* expression and *lncIRF8* transcription in pDC (purple wavy lines). This negative feedback inhibition of IRF8 on the +32 kb enhancer allows *IRF8* to regulate its own expression and thus DC differentiation. *lncIRF8* expression by RNA-seq and IRF8 binding by ChIP-seq in cDC and pDC are shown. The RNA-seq and IRF8 ChIP-seq data are shown as in Figure 1A, Figure S1, and Figure S4A.

(B) Recapitulating *IRF8* and *lncIRF8* transcription by repression and activation of the *IRF8* +32 kb enhancer in HoxB8 MPP by targeted dCas9-KRAB and dCas9-VP64, respectively. Green and purple wavy lines represent gene expression as described in Figure 5A and Figure 6A.